





PI3KC2 β inactivation stabilizes VE-cadherin junctions and preserves vascular integrity

Typhaine Anquetil^{1,†} , Romain Solinhac^{1,†}, Aude Jaffre¹, Gaëtan Chicanne¹, Julien Viaud¹ , Jean Darcourt¹, Cyrille Orset², Eva Geuss³ , Christoph Kleinschnitz⁴, Bart Vanhaesebroeck⁵ , Denis Vivien^{2,6}, Karim Hnia¹, Vincent Larrue^{1,7}, Bernard Payrastre^{1,8} & Marie-Pierre Gratacap^{1,*} 

Abstract

Endothelium protection is critical, because of the impact of vascular leakage and edema on pathological conditions such as brain ischemia. Whereas deficiency of class II phosphoinositide 3-kinase alpha (PI3KC2 α) results in an increase in vascular permeability, we uncover a crucial role of the beta isoform (PI3KC2 β) in the loss of endothelial barrier integrity following injury. Here, we studied the role of PI3KC2 β in endothelial permeability and endosomal trafficking *in vitro* and *in vivo* in ischemic stroke. Mice with inactive PI3KC2 β showed protection against vascular permeability, edema, cerebral infarction, and deleterious inflammatory response. Loss of PI3KC2 β in human cerebral microvascular endothelial cells stabilized homotypic cell–cell junctions by increasing Rab11-dependent VE-cadherin recycling. These results identify PI3KC2 β as a potential new therapeutic target to prevent aggravating lesions following ischemic stroke.

Keywords endosomal trafficking; endothelial hyperpermeability; phosphoinositide 3-kinase C2 β ; vascular biology; vascular endothelial-cadherin

Subject Categories Cell Adhesion, Polarity & Cytoskeleton; Molecular Biology of Disease; Vascular Biology & Angiogenesis

DOI 10.15252/embr.202051299 | Received 10 July 2020 | Revised 2 March 2021 | Accepted 12 March 2021 | Published online 20 April 2021

EMBO Reports (2021) 22: e51299

Introduction

After ischemia, such as in stroke, tissue injury is often exacerbated upon reperfusion (Hacke *et al*, 2008; Esenwa & Gutierrez, 2015; Yang *et al*, 2019). This is due to an inflammatory response mediated by cytokines (e.g., tumor necrosis factor α [TNF α] (Lambertsen

et al, 2019), interleukin [IL]-1 β (Yang *et al*, 2019), and IL-6 (Lambertsen *et al*, 2019)), that can rupture the endothelial barrier. The tightness of intercellular junctions, particularly adherens junctions composed of vascular endothelial (VE)-cadherin-mediated homotypic cell–cell adhesion, is a key determinant of vascular permeability (Dejana & Vestweber, 2013; Giannotta *et al*, 2013; Wessel *et al*, 2014) associated with leukocyte infiltration, edema, and secondary cerebral hemorrhage complications. Thus, controlling the levels of VE-cadherin at the adherens junctions is of potential therapeutic interest.

Like many cell surface receptors, VE-cadherin traffics through the endosomal system, an intracellular vesicular network controlled partly by the interconversion of phosphoinositide lipids. In particular, the intracellular membrane lipid messenger, phosphatidylinositol 3-phosphate (PI3P) produced by the class II phosphoinositide 3-kinase alpha (PI3KC2 α), is known to control vesicular trafficking required for normal delivery of cell surface proteins (Yoshioka *et al*, 2012; Posor *et al*, 2013; Campa *et al*, 2018; Bilanges *et al*, 2019; Gulluni *et al*, 2019). PI3KC2 α gene deletion in mice is embryonically lethal, because of abnormal angiogenesis and a defect in the maintenance of vascular barrier integrity in quiescent vessels (Yoshioka *et al*, 2012). However, the deletion or inactivation of PI3KC2 β enzymatic activity in mice expressing a catalytically inactive form of PI3KC2 β does not affect viability, nor leads to any particular phenotype (Harada *et al*, 2005). Therefore, the role of PI3KC2 β remains largely unknown (Nigorikawa *et al*, 2014; Marat *et al*, 2017). PI3KC2 β depletion has been shown to decrease the adhesion and migration of endothelial (Tibolla *et al*, 2013) and cancer cells (Chikh *et al*, 2016; Mavrommati *et al*, 2016). When endogenous PI3KC2 β is converted into a kinase-dead allele in mice, they demonstrate enhanced insulin sensitivity and protection against high-fat diet-induced hepatic steatosis (Alliouachene *et al*, 2015). Therefore, targeting PI3KC2 β could be beneficial in several pathological contexts.

- INSERM, UMR-S U1297 and University of Toulouse III, Institute of Cardiovascular and Metabolic Diseases (I2MC), CHU-Rangueil, Toulouse, France
- INSERM, UMR-S U1237 and Caen-Normandie University, Physiopathology and Imaging of Neurological Disorders (PhIND), GIP Cyceron, Caen, France
- Department of Neurology, University of Würzburg, Würzburg, Germany
- Department of Neurology, Essen University Hospital, Essen, Germany
- Cell Signaling, UCL Cancer Institute, University College London, London, UK
- CHU Caen, Department of Clinical Research, Caen University Hospital, Caen, France
- Department of Neurology, University Hospital of Toulouse, Toulouse, France
- Laboratoire d'Hématologie, CHU de Toulouse, Toulouse Cedex, France

*Corresponding author. Tel: +33 05 61 32 56 00; E-mail: marie-pierre.gratacap@inserm.fr

†These authors contributed equally to this work

Here, we explored the role of PI3KC2 β in the preservation of endothelial integrity in ischemic stroke, *in vitro* and *in vivo*, and uncover a crucial and unexpected role of this isoform. Mice expressing an inactive PI3KC2 β (PI3KC2 β kinase-dead mice) show robust neuroprotection by preserving the blood–brain barrier (BBB) from ischemic injury in two models of stroke with reperfusion (transient middle cerebral artery occlusion [tMCAO] and thromboembolic stroke). Interestingly, we reveal here that PI3KC2 β is critical in maintaining cerebral endothelial integrity by controlling endosomal trafficking of VE-cadherin. We show that PI3KC2 β deletion in human cerebral microvascular endothelial cells preserves VE-cadherin stability at adherens junctions. Indeed, PI3KC2 β loss decreases a specific pool of PI3P in the endosomal compartment of these cells, affecting the early endosomal maturation and favoring endosomal recycling. Our results demonstrate for the first time that inactivating PI3KC2 β promotes junction reannealing at the endothelial cell membrane in the context of thromboinflammation in stroke. These results indicate that the inhibition of PI3KC2 β could be an interesting therapeutic strategy to improve the outcome of this devastating condition.

Results

PI3KC2 β inactivation preserves endothelial junction integrity in experimental stroke models

To gain insight into the role of PI3KC2 β in endothelium integrity *in vivo*, we used transgenic mice expressing a catalytically inactive form of PI3KC2 β (hereafter called C2 β ^{D1212A/D1212A} mice), mimicking the full inactivation of PI3KC2 β at the organismal level. These mice exhibit unaltered endogenous expression of the inactive PI3KC2 β protein and of other PI3K isoforms (Alliouachene *et al.*, 2015).

Cerebrovascular permeability of WT and C2 β ^{D1212A/D1212A} mice was analyzed using a tMCAO model, with 1 h of occlusion (Appendix Fig S1A) (Braeuninger *et al.*, 2012) followed by 24 h of reperfusion, by quantifying vascular leakage of Evans blue dye into the brain parenchyma. As shown in Fig 1A, vascular leakage was significantly lower in C2 β ^{D1212A/D1212A} mice compared to WT mice (34.06 \pm 7.93 mm³ for WT vs 8.95 \pm 6.59 for C2 β ^{D1212A/D1212A} mice). We also found a significant reduction in brain edema (9.26% \pm 0.85% for WT vs 6.27 \pm 0.68 for C2 β ^{D1212A/D1212A}; Fig 1A) indicating that the BBB integrity was preserved. Moreover, 2,3,5-triphenyltetrazolium chloride (TTC) staining of the brain sections (Fig 1B) showed a significant decrease (51%) in infarct volume in C2 β ^{D1212A/D1212A} compared to WT mice. Notably, this phenotype was intermediate in heterozygous PI3KC2 β kinase-dead mice (C2 β ^{WT/D1212A}; 32.2%), underscoring a dose-dependent contribution of PI3KC2 β activity in this process. Consistent with these data, C2 β ^{D1212A/D1212A} mice displayed increased survival rates (Fig 1C), improved global neurological function 24 h after tMCAO (Bederson score: mean, 2.82 for WT vs 2.04 for C2 β ^{D1212A/D1212A}), and improved motor function and coordination (grip test: mean, 2.26 for WT vs 3.07 for C2 β ^{D1212A/D1212A}; Fig 1D).

C2 β ^{D1212A/D1212A} mice were then submitted to the thromboembolic stroke model, consisting of an *in situ* induction of occlusive thrombus in the middle cerebral artery (MCA) via direct intra-arterial injection of recombinant α -thrombin (Appendix Fig S1B) (Orset

et al., 2007). As observed in Appendix Fig S3, cerebral blood flow (CBF) was comparable in WT and C2 β ^{D1212A/D1212A} mice before (baseline CBF, $t = 0$) and up to 1 h ($t = 60$) after α -thrombin injection. Infarct volume was measured 24 h post- α -thrombin injection by magnetic resonance imaging (MRI). As shown in Fig 1E, PI3KC2 β inactivation led to a significant reduction (32.67%) in ischemic lesion size. Given the fact that angiogenesis can protect the brain against ischemic injury (Xiong *et al.*, 2010), we checked whether the suppression of PI3KC2 β catalytic activity would affect vessel density. As shown in Appendix Fig S2, isolectin B4 staining of brain sections revealed comparable vessel densities in the cortex or basal ganglia from WT and C2 β ^{D1212A/D1212A} mice. These results show that PI3KC2 β inactivation significantly reduced injuries in two different stroke models in mice without modifying vessel density.

Brain inflammation is reduced in C2 β ^{D1212A/D1212A} mice

Pro-inflammatory mediator production is known to increase in patients at stroke onset, reinforcing the expression of cytokines and adhesion molecules driving infiltration of neutrophils into the ischemic tissue and BBB damage (Konsman *et al.*, 2007; Iadecola & Anrather, 2011). Quantitative transcript analysis of the prototypic pro-inflammatory cytokines TNF α , IL-1 β , and IL-6 was performed 24 h after tMCAO and revealed a marked decrease in mRNA levels in the ischemic (ipsilateral) cortex (TNF α : 74.8%, IL-1 β : 87.8%, and IL-6: 69.7%) and basal ganglia (TNF α : 57.3%, IL-1 β : 78.1%, and IL-6: 36.2%) of C2 β ^{D1212A/D1212A} compared to WT mice brains (Fig 2A). Similar results were obtained at the protein level (Fig 2B). Neutrophil extravasation was also lower in the ischemic hemisphere of these mice (Fig 2C), indicating that PI3KC2 β inactivation efficiently reduced brain inflammation. Of note, no intracranial hemorrhage was observed in C2 β ^{D1212A/D1212A} mice after tMCAO.

To evaluate the degree of endothelial cell activation *in vivo*, we used ultrasensitive molecular MRI to monitor cerebrovascular inflammatory molecule expression, such as the adhesion molecule P-selectin (Quenault *et al.*, 2017). Antibody-coated microsized particles of iron oxide (MPIOs) targeting P-selectin were intravenously injected into mice 24 h after induced acute thrombosis in the MCA. MRI acquisition was performed 20 min after the administration of targeted MPIOs. C2 β ^{D1212A/D1212A} mice expressed significantly less endothelial P-selectin compared to WT mice (2.26% vs 5.18%), providing evidence for reduced endovascular inflammation (Fig 2D).

PI3KC2 β inactivation protects against reperfusion lesions

We thought to determine whether PI3KC2 β inactivation hindered the effect of ischemia, or prevented reperfusion lesions, or both. For this, we quantified transcript levels of inflammatory markers after 1 h of ischemia as a readout of brain lesion which, *per se*, was not yet detectable using classical approaches. TNF α expression and IL-1 β expression were both higher in WT and C2 β ^{D1212A/D1212A} ischemic brain hemispheres after 1-h ischemia and in the absence of reperfusion, indicating a comparable degree of inflammation in both genotypes (Fig 3A, upper right panel). Of note, IL-6 expression and VCAM-1 expression were undetectable after 1-h ischemia without reperfusion in WT and C2 β ^{D1212A/D1212A} mice (Fig 3A, bottom right

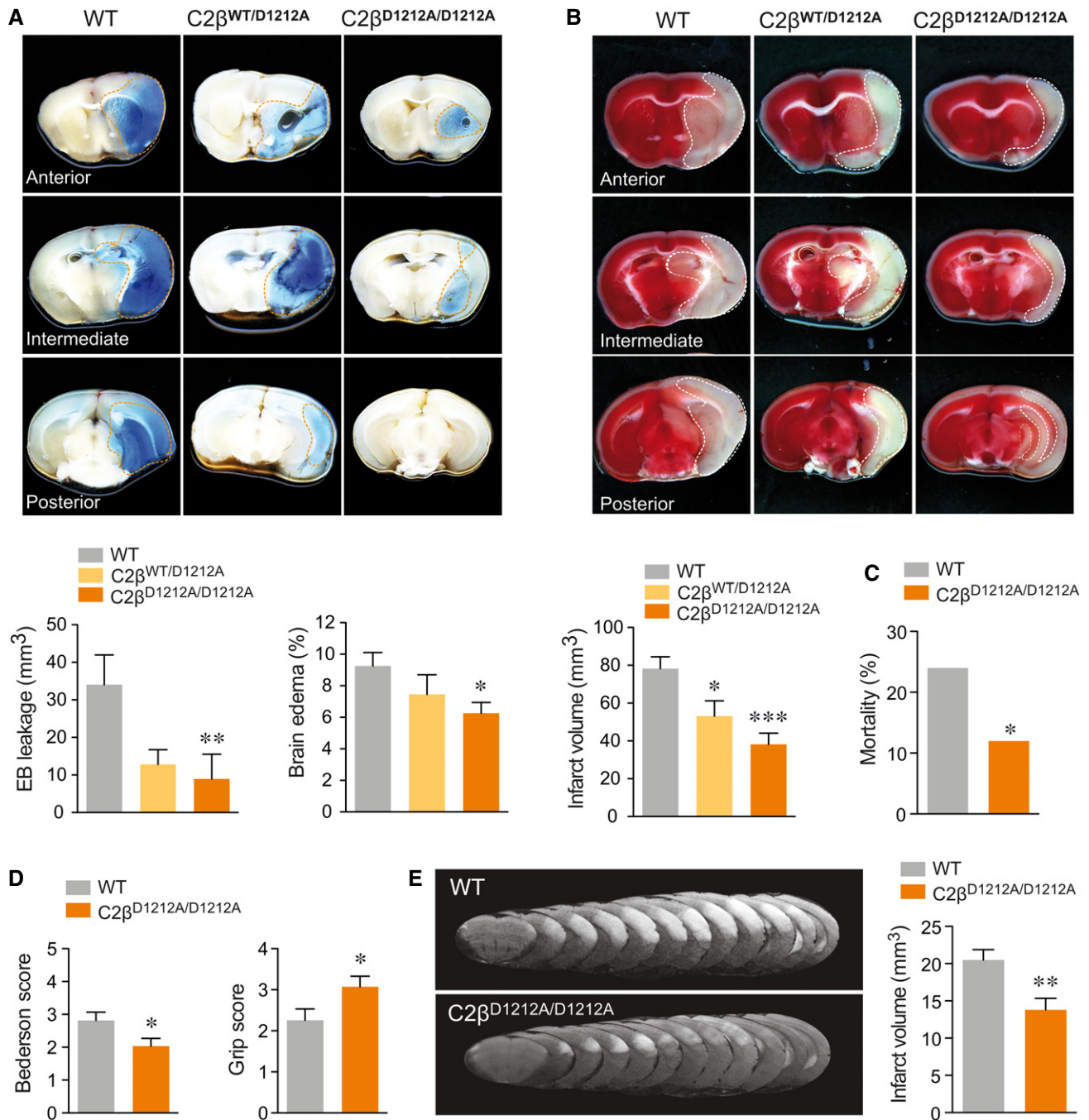


Figure 1. Genetic inhibition of PI3K C2β reduces vascular leakage, edema, and cerebral infarction and improves neurological outcomes in ischemia/reperfusion stroke models.

A–D WT, heterozygous (C2β^{WT/D1212A}) and C2β^{D1212A/D1212A} mice were subjected to tMCAO (1 h ischemia followed by 24 h reperfusion). (A) Representative photographs of coronal brain sections and graph quantification of Evans blue (EB) dye leakage (dashed orange line) and edema volume. Data represent mean ± SEM (EB leakage: *n* = 5–16 mice per group; edema volume: *n* = 14–30 mice per group; **P* < 0.05, ***P* < 0.01 Mann–Whitney test). (B) Representative photographs of coronal brain section stained with TTC (dashed white line) and graph quantification of infarct volume measurements. Data represent mean ± SEM (*n* = 14–27 mice per group; **P* < 0.05; ****P* < 0.001, unpaired *t*-test). (C) Mortality between day 0 and day 1 after reperfusion by tMCAO (*n* = 30–39 mice per group; **P* < 0.05, Fisher’s test). (D) Neurological scores evaluated 24 h after reperfusion by Bederson test (left panel) and grip test (right panel) based on a five point system. Data represent mean ± SEM (*n* = 14–27 mice per group; **P* < 0.05, unpaired *t*-test).

E WT and C2β^{D1212A/D1212A} mice were subjected to thromboembolic stroke model. Representatives T2-weighted MRI of coronal section taken 24 h after the onset of *in situ* clot formation by α-thrombin are shown. Graph quantification of infarct volume measurements. Data represent mean ± SEM (*n* = 23–25 mice per group; ***P* < 0.01, unpaired *t*-test).

Source data are available online for this figure.

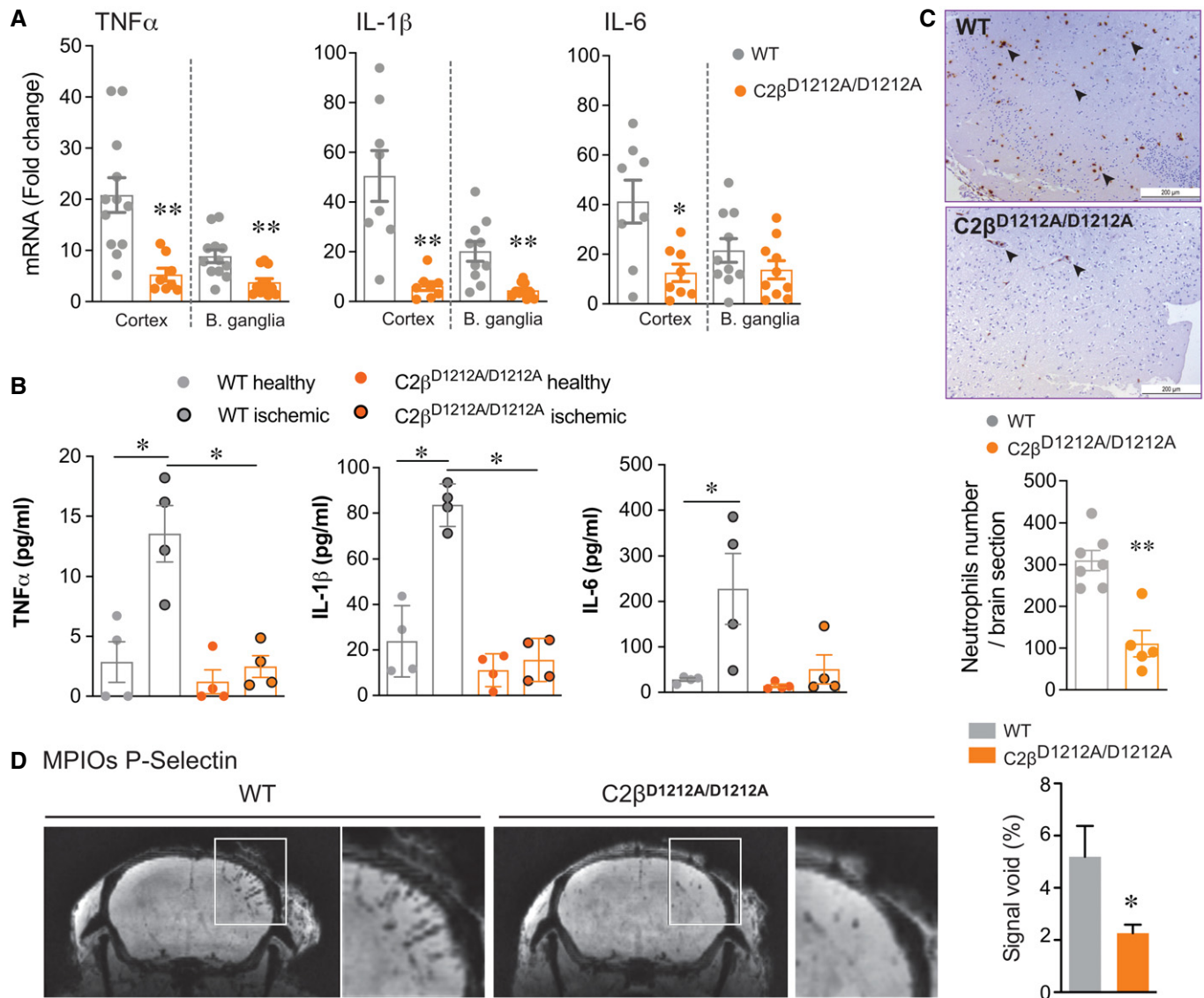


Figure 2. Genetic inhibition of PI3KC2 β reduces inflammation 24 h after stroke.

A–C WT and $C2\beta^{D1212A/D1212A}$ mice were subjected to tMCAO followed by 24 h of reperfusion. (A) Gene expression of $TNF\alpha$, $IL-1\beta$, and $IL-6$ in the cortex and basal ganglia (B. ganglia). The mRNA levels are given as the fold change normalized to rps29 relative to the corresponding contralateral (healthy) hemisphere. Data represent mean \pm SEM ($n = 8$ –10 mice per group; * $P = 0.05$ and ** $P < 0.01$, unpaired t -test with Welch's correction). (B) Protein expression of $TNF\alpha$, $IL-1\beta$, and $IL-6$. Data represent mean \pm SEM ($n = 4$ mice per group; * $P = 0.05$; Mann–Whitney test). (C) Representative immunohistochemistry of neutrophils (arrowheads) in ischemic hemisphere (scale bar 200 μm) and graph quantification. Data represent mean \pm SEM ($n = 5$ –7 mice per group; ** $P < 0.01$; Mann–Whitney test).

D Representative T2-weighted MRI of WT and $C2\beta^{D1212A/D1212A}$ mice taken 24 h after clot formation and graph quantification of area stained by P-selectin using MPIOs in ipsilateral (ischemic) normalize to contralateral (healthy) cortex in percentage. Data represent mean \pm SEM ($n = 10$ –11 mice per group; * $P < 0.05$; unpaired t -test with Welch's correction).

Source data are available online for this figure.

panel). However, 4 h after reperfusion, their expression increased in the ischemic brain hemisphere of WT mice, while it remained low in $C2\beta^{D1212A/D1212A}$ mice (Fig 3A, bottom left panel). The differences were sustained over a course of 24 h post-reperfusion (Fig 2A).

Another strategy to evaluate the effect of PI3KC2 β inactivation in the absence of reperfusion was to measure infarct volume after permanent MCAO (pMCAO) by electrocoagulation. Here, PI3KC2 β inactivation failed to reduce the size of the ischemic lesion (Fig 3B), suggesting that its neuroprotective effects were largely related to

arterial recanalization, rather than a specific neuroprotective function against ischemia. Overall, these results indicate that PI3KC2 β inactivation protects against reperfusion injury.

Inhibition of PI3KC2 β in the hematopoietic compartment is not essential for BBB protection *in vivo*

To assess the potential contribution of hematopoietic PI3KC2 β , we generated bone marrow (BM) chimeras by reconstitution of sublethally

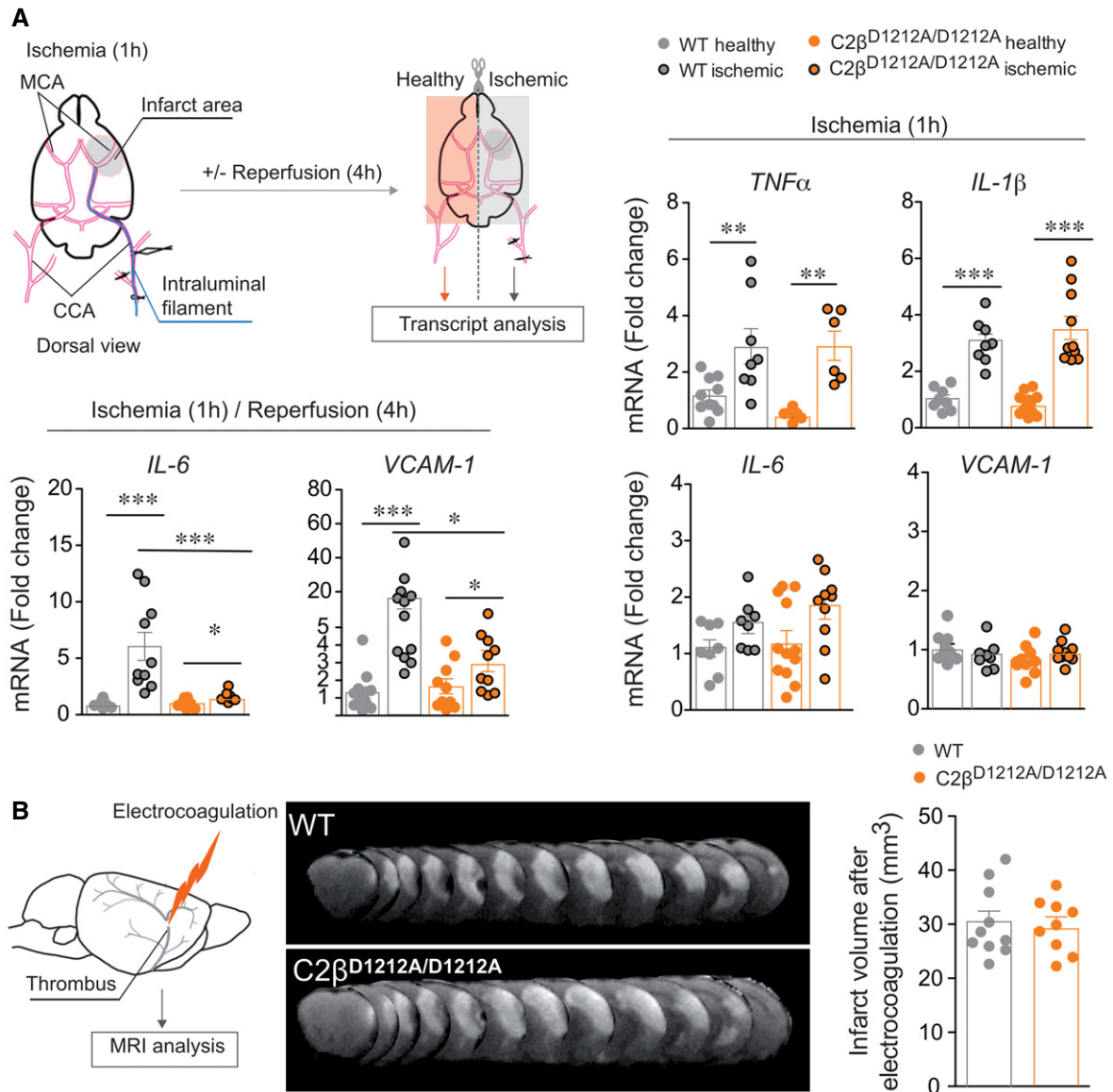


Figure 3. In the absence of reperfusion, genetic inhibition of PI3KC2β does not affect inflammatory cytokine profile and infarct volume.

A Gene expression of *TNFα* ($n = 8-10$ mice for WT and $n = 6$ mice for $C2\beta^{D1212A/D1212A}$), *IL-1β* ($n = 8$ mice for WT and $n = 10-12$ mice for $C2\beta^{D1212A/D1212A}$), *IL-6* ($n = 8$ mice for WT and $n = 10-12$ mice for $C2\beta^{D1212A/D1212A}$), and *VCAM-1* ($n = 8-10$ mice for WT and $n = 10$ mice for $C2\beta^{D1212A/D1212A}$) after 1 h of ischemia without reperfusion (right panel). Gene expression of *IL-6* ($n = 10-12$ mice for WT and $n = 8$ mice for $C2\beta^{D1212A/D1212A}$) and *VCAM-1* ($n = 12$ mice for WT and $n = 10$ mice for $C2\beta^{D1212A/D1212A}$) after 1 h of ischemia followed by 4 h of reperfusion (bottom, left panel) on WT and $C2\beta^{D1212A/D1212A}$ mice. The mRNA levels are given as the fold increase normalized to PGK1 relative to the healthy contralateral hemisphere of WT mice. Data represent mean \pm SEM (*** $P < 0.001$, ** $P < 0.01$, and * $P < 0.05$, Mann-Whitney test or unpaired t -test, as accordance).

B Representative photographs of T2-weighted MRI of WT and $C2\beta^{D1212A/D1212A}$ mice and graph quantification of ischemic lesion after 24 h permanent MCAO (electrocoagulation model). Data represent mean \pm SEM ($n = 9-10$ mice per group; ns, unpaired t -test).

Source data are available online for this figure.

irradiated WT mice with BM harvested from $C2\beta^{D1212A/D1212A}$ or WT mice and vice versa. Gene amplification from BM homogenates confirmed the expected PI3KC2β genotype in the hematopoietic cells from chimeric mice (Appendix Fig S4A). Platelet count was not significantly affected by the graft, suggesting normal hematopoiesis (Appendix Fig S4B). As shown in Fig 4A, transplantation of $C2\beta^{D1212A/D1212A}$ BM into WT hosts ($C2\beta^{D1212A} > WT$) did not

significantly affect the infarct size 24 h after reperfusion compared to mice receiving WT BM (WT > WT). However, we observed significant protection associated with reduced brain edema when WT BM was transplanted into $C2\beta^{D1212A/D1212A}$ recipients (WT > $C2\beta^{D1212A}$). It indicates that non-hematopoietic PI3KC2β plays a major role in the protection against ischemic stroke lesions (Fig 4A and B). Consistent with these results, when platelet activation was specifically assessed,

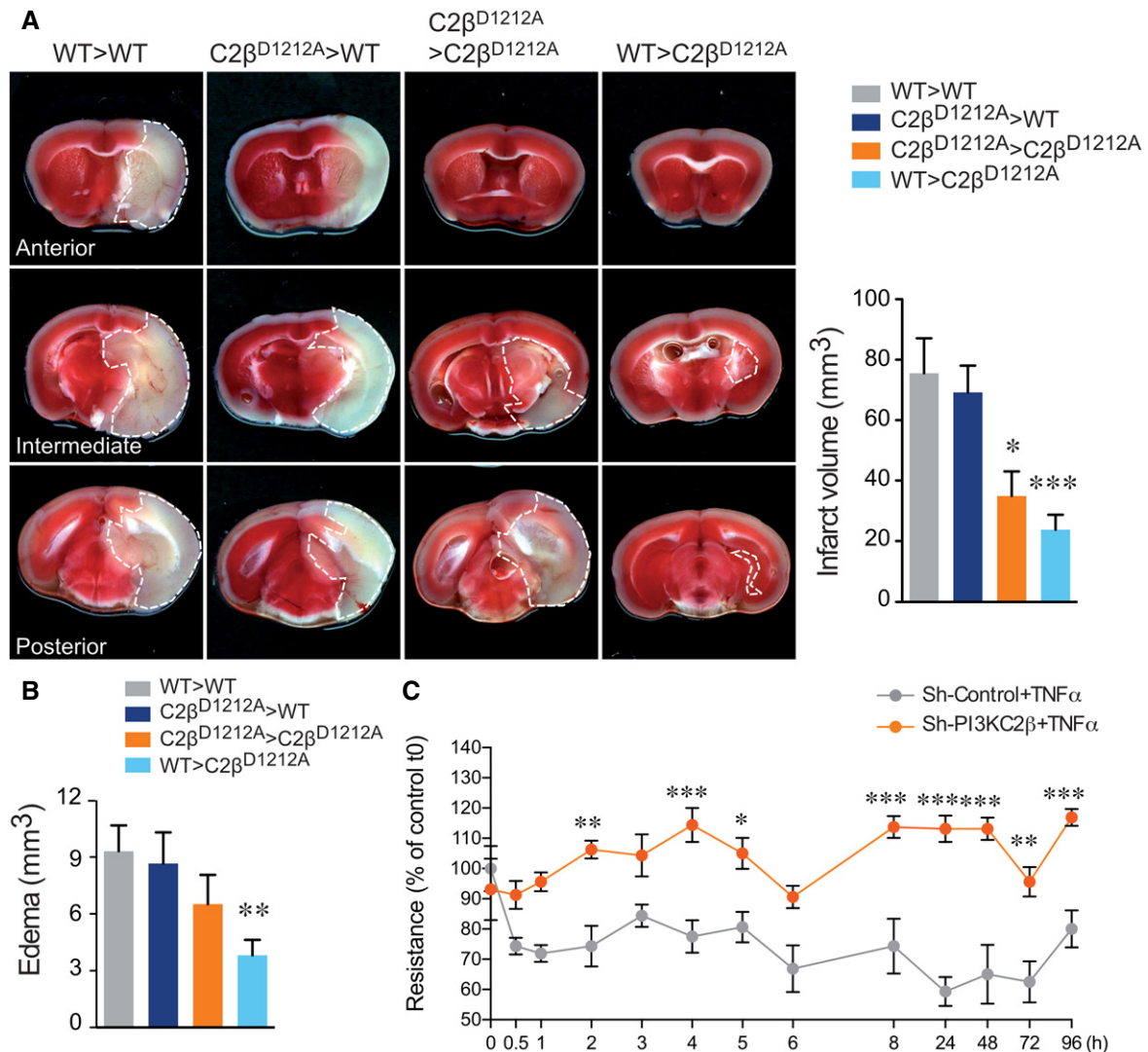


Figure 4. PI3KC2β inactivation in the non-hematopoietic compartment reduces cerebral infarction and edema *in vivo* and preserves endothelial barrier integrity *in vitro*.

A, B Representative photographs of coronal brain sections and graph quantification of infarct volume (dashed white line) measurements (A) and edema volume (B) in bone marrow (BM) chimeric mice 24 h after tMCAO. WT > WT: transplantation of WT BM into WT hosts; C2β^{D1212A} > WT: transplantation of C2β^{D1212A/D1212A} BM into WT hosts; C2β^{D1212A} > C2β^{D1212A}: transplantation of C2β^{D1212A/D1212A} BM into C2β^{D1212A/D1212A} hosts; and WT > C2β^{D1212A}: transplantation of WT BM into kinase-dead hosts. Data represent mean ± SEM; *n* = 13–16 mice per group; **P* < 0.05; ***P* < 0.01; ****P* < 0.001 vs WT > WT, Mann–Whitney test or unpaired *t*-test, as accordance.

C Sh-control or sh-PI3KC2β hCMEC/D3 cells were cultured on Transwell and stimulated with TNFα over the time. Trans-endothelial electrical resistance (TEER) was measured with a voltohmmeter Millicell ERS-2 at the indicated time. Data are shown in percentage of control at t0 ± SEM (*n* = 4 independent experiments). ****P* < 0.001; ***P* < 0.01; **P* < 0.05, significance differences from control, two-way ANOVA with Bonferroni post-test.

Source data are available online for this figure.

we found that C2β^{D1212A/D1212A} mice had normal platelet aggregation response and tail bleeding time, indicating that the absence of PI3KC2β activity spared activation of these anucleate cells (Appendix Fig S4C and D). Collectively, these results indicate that the marked reduction of infarct volume in C2β^{D1212A/D1212A} mice is not due to the hematopoietic tissue, suggesting the implication of the endothelial compartment.

To explore the direct implication of PI3KC2β in endothelial cell–cell junction stability, we knocked down PI3KC2β in the

human cerebral microvascular endothelial hCMEC/D3 cell line (Weksler *et al*, 2005; Daniels *et al*, 2013; Weksler *et al*, 2013) using short hairpin RNAs (Appendix Fig S5A) and performed trans-endothelial electrical resistance (TEER) across a monolayer of endothelial cells (EC). As expected, control cells cultured on Transwell inserts and stimulated with TNFα (Chaitanya *et al*, 2011) for 96 h resulted in paracellular permeability (Fig 4C). In contrast, PI3KC2β depletion significantly preserved the endothelial barrier integrity, as revealed by a stable TEER. These results

indicate that PI3KC2 β inhibition stabilizes the EC barrier both *in vivo* and *in vitro*.

PI3KC2 β knockdown causes an expansion of very early and recycling endosomes in human cerebral microvascular endothelial cells

We then investigated the molecular mechanisms linking PI3KC2 β inhibition and the regulation of cell–cell junction organization in ECs. As shown in Appendix Fig S5A and Fig 6A, shRNAs induced a significant reduction in PI3KC2 β protein level with unaltered expression of class II PI3KC2 α . Of note, cell viability, proliferation, and growth factor signaling (Appendix Figs S5B and C, and S6B) were not affected by shRNA-mediated PI3KC2 β knockdown. This indicates that this kinase is not involved in the regulation of these key processes. Moreover, PI3KC2 β is not implicated in the mTORC pathway regulation in our model, as recently proposed in HeLa cells submitted to serum restriction (Marat *et al*, 2017) (Appendix Fig S6C).

We first analyzed transferrin uptake and recycling, a key processes in which PI3K products have been implicated. Knockdown of PI3KC2 β displayed a significant decrease (43.6%) in transferrin endocytosis after 5 min of uptake (Fig 5A) indicating that PI3KC2 β is involved in endocytosis in hCMEC/D3 cells. Furthermore, we observed faster transferrin recycling in PI3KC2 β -depleted cells supporting a model where the absence of PI3KC2 β also promotes also the endosomal recycling route. Results show that following 20 min of transferrin uptake, there is a 10% decrease in internalized transferrin in control cells versus 45.5% decrease in PI3KC2 β -depleted cells indicating a higher transferrin recycling/exocytosis in knockdown cells (Fig 5A). These data indicate that PI3KC2 β knockdown affects both, endocytosis and recycling, mechanisms in hCMEC/D3.

Furthermore, analysis of the different endosomes by confocal microscopy showed that PI3KC2 β depletion in hCMEC/D3 cells increased the number, but not the size, of very early endosomes (VEEs; APPL1 positives) and of recycling endosomes (Rab11a positives), both in untreated and TNF α -treated cells (Fig 5B–D and Appendix Fig S7), strengthening the idea that in the absence of PI3KC2 β , the recycling path was increased. This effect was not specific to the hCMEC/D3 cell line because similar results were obtained in another human microvascular endothelial cell line (HMEC-1; Appendix Fig S8A and B). This increase correlated with a decrease in the number and size of early endosomes (EEs; EEA1 positives) and late endosomes/lysosomes (LAMP1), suggesting the role of PI3KC2 β in the maturation of VEEs to EE (Fig 5C and D). Coinciding with immunofluorescence experiments, subcellular fractionation of endosomal compartments in cell homogenates showed APPL1- and Rab11a-positive endosomal fraction amelioration in PI3KC2 β -depleted cells, with a decrease in EEA1- and Rab5-positive endosome fractions, whereas the level of Rab7, a marker of late endosome, was unchanged (Appendix Fig S9).

We then investigated the activity of the small GTPases Rab11, Rab7, and Rab5, a GTPase implicated in the APPL1/EEA1 interconversion (Zoncu *et al*, 2009) (Fig EV1A). We found that the level of GTP-loaded Rab5 and Rab7 was not affected by the absence of PI3KC2 β . However, the GTP-bound form of Rab11 was

significantly higher in PI3KC2 β -knockdown cells compared to control (Fig EV1A). This effect was not due to Rab11 overexpression since the expression level of Rab5, Rab7, and Rab11 proteins in the total cell lysate was not affected by the absence of PI3KC2 β (Fig EV1B). Since we also observed an increase in Rab11 protein level in the endosomal compartment of PI3KC2 β -knockdown cells (Fig 5C and Appendix Fig S9), we can reasonably suggest that Rab11 activity was increased in this compartment. Overall, these results suggest that the absence of PI3KC2 β favors the recycling pathway in these cells by increasing Rab11 activity and its presence in endosomes.

PI3KC2 β knockdown stabilizes cell–cell junctions by promoting the VE-cadherin recycling path

To assess whether disrupted endosomal trafficking impacts cell–cell junctions, we monitored the presence of VE-cadherin on the surface of ECs as readout of junction opening. In control cells, a 24-h treatment with TNF α significantly reduced VE-cadherin at cell–cell contacts compared to resting cells, revealing the paracellular junction-opening property of this cytokine (Fig 6A). Intriguingly, PI3KC2 β -depleted cells exhibited much higher levels of VE-cadherin at adherens junctions, and VE-cadherin levels were not significantly affected by the addition of TNF α (Fig 6A and Appendix Fig S10A). Accordingly, high VE-cadherin levels were also found when cells were cultured in oxygen–glucose deprivation (OGD) conditions, mimicking the effects of ischemia (Fig 6B). Thus, the knockdown of PI3KC2 β preserved paracellular integrity by promoting the accumulation and maintenance of VE-cadherin at junctions. This result was validated by Western blot analysis, demonstrating higher total amount of VE-cadherin present in cell lysate in the absence of PI3KC2 β (+46.4% in resting PI3KC2 β -knockdown cells compared to control cells; Fig 6C) while the mRNA level remains unchanged (Fig 6D) suggesting that the absence of PI3KC2 β interferes with VE-cadherin degradation.

We then determined the amount of PI3KC2 β lipid products in these cells by imaging with the well-characterized FYVE^(HRS) PI3P probe and the PH^(TAPP1) PI(3,4)P₂ probe. Results showed that the knockdown of PI3KC2 β did not modify PI(3,4)P₂ level on endomembranes but induced a 38% loss of PI3P compared to control cells (Fig 7A) and this difference persisted after TNF α stimulation (Appendix Fig S10B). The decrease in basal PI3P was further confirmed by a specific PI3P mass assay (Chicanne *et al*, 2012), allowing the total amount of cellular PI3P to be measured (45.36% decrease in resting sh-PI3KC2 β compared to sh-control cells; Fig 7B). Of note, determination of PI3P localization on endomembranes shows a strong colocalization of PI3P with EEA1 but not with APPL1, Rab11, and LAMP1 in sh-control and sh-PI3KC2 β cells (Appendix Fig S11A and B). Interestingly, a decrease in Manders overlap coefficient of PI3P on EEA1-positive endosomes was observed (0.3858 \pm 0.02 for sh-control cells versus 0.3191 \pm 0.023 for sh-PI3KC2 β cells) suggesting that PI3KC2 β may produce a pool of PI3P on EEA1 early endosomes.

We then evaluated the contribution of Vps34, the major PI3P-synthesizing enzyme, on PI3P level in control and PI3KC2 β -knockdown hCMEC/D3 cells, by using a specific inhibitor, IN1. Results show that IN1 (1 μ M) decreased PI3P level by about 66% in control cells, whereas inhibition of both, Vps34 and

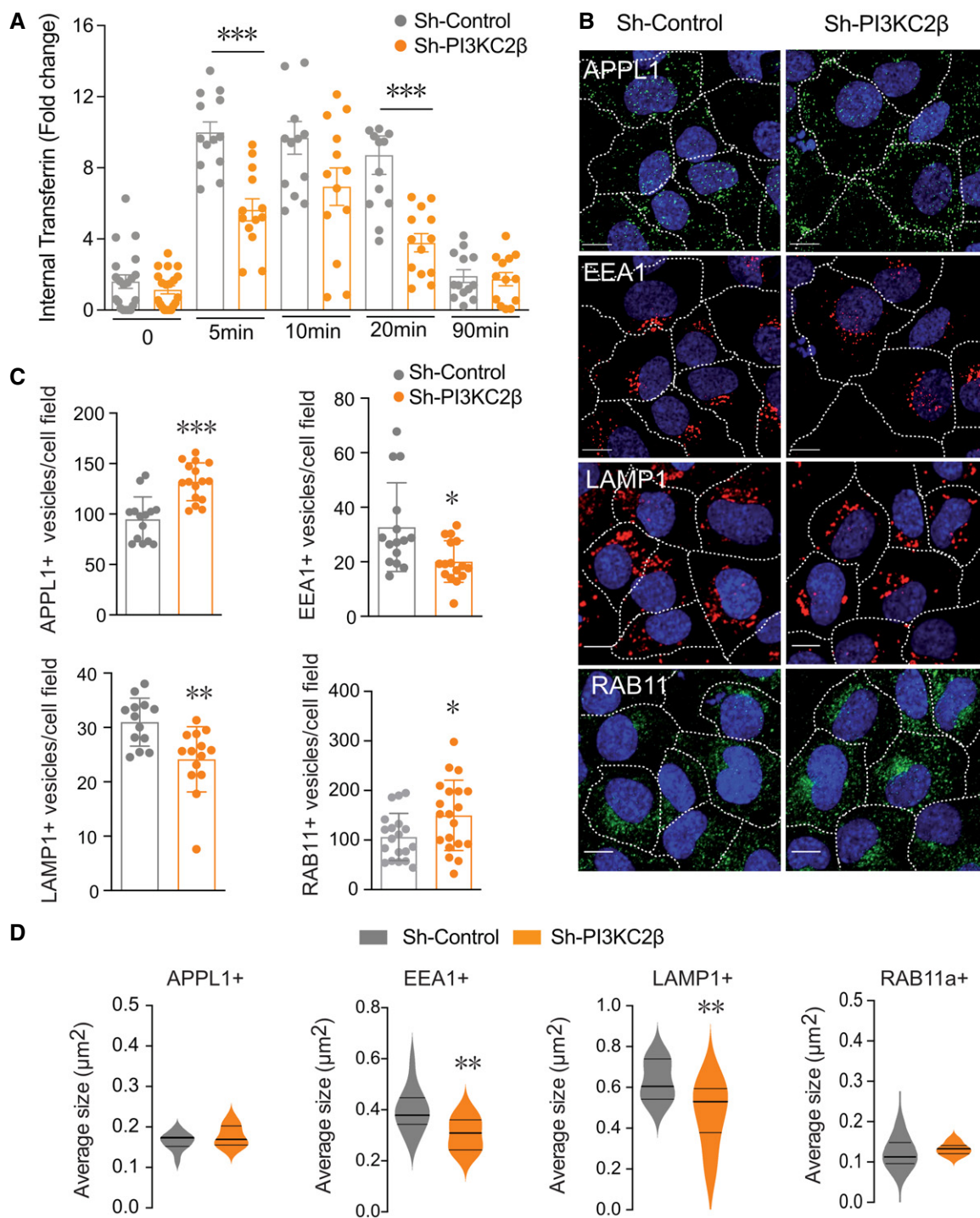


Figure 5. PI3KC2 β depletion disturbs endosomal trafficking with increase of VEE (APPL1⁺) and recycling (Rab11a⁺) endosomes.

- A** Quantification of internal transferrin in sh-control or sh-PI3KC2 β cells at different incubation time points (ImageJ software). Results are expressed as fold change of internalized Alexa Fluor[®]546-transferrin. Data represent mean \pm SEM of cell fields randomly selected (dots $n = 13$ – 20). Data are collected from 4 independent experiments. *** $P < 0.001$ Mann–Whitney test.
- B** Analysis of APPL1, EEA1, LAMP1, and Rab11a staining in sh-control and sh-PI3KC2 β hCMEC/D3 cells. White dotted lines delineate cells; scale bar, 10 μ m; nuclei are shown in blue (DAPI).
- C, D** Quantification was performed to determine number (C) and average size (D) of positive vesicles per cell (ImageJ software). Nuclei are shown in blue (DAPI). Data represent mean \pm SEM of cell fields randomly selected ($n = 13$ – 20 for (C) and $n = 11$ – 20 for (D)). Data are collected from at least 3–4 independent experiments. For violin plots (D), thick lines represent median and thin lines interquartile; *** $P < 0.001$; ** $P < 0.01$; * $P < 0.05$, unpaired t -test or Mann–Whitney, as accordance.

Source data are available online for this figure.

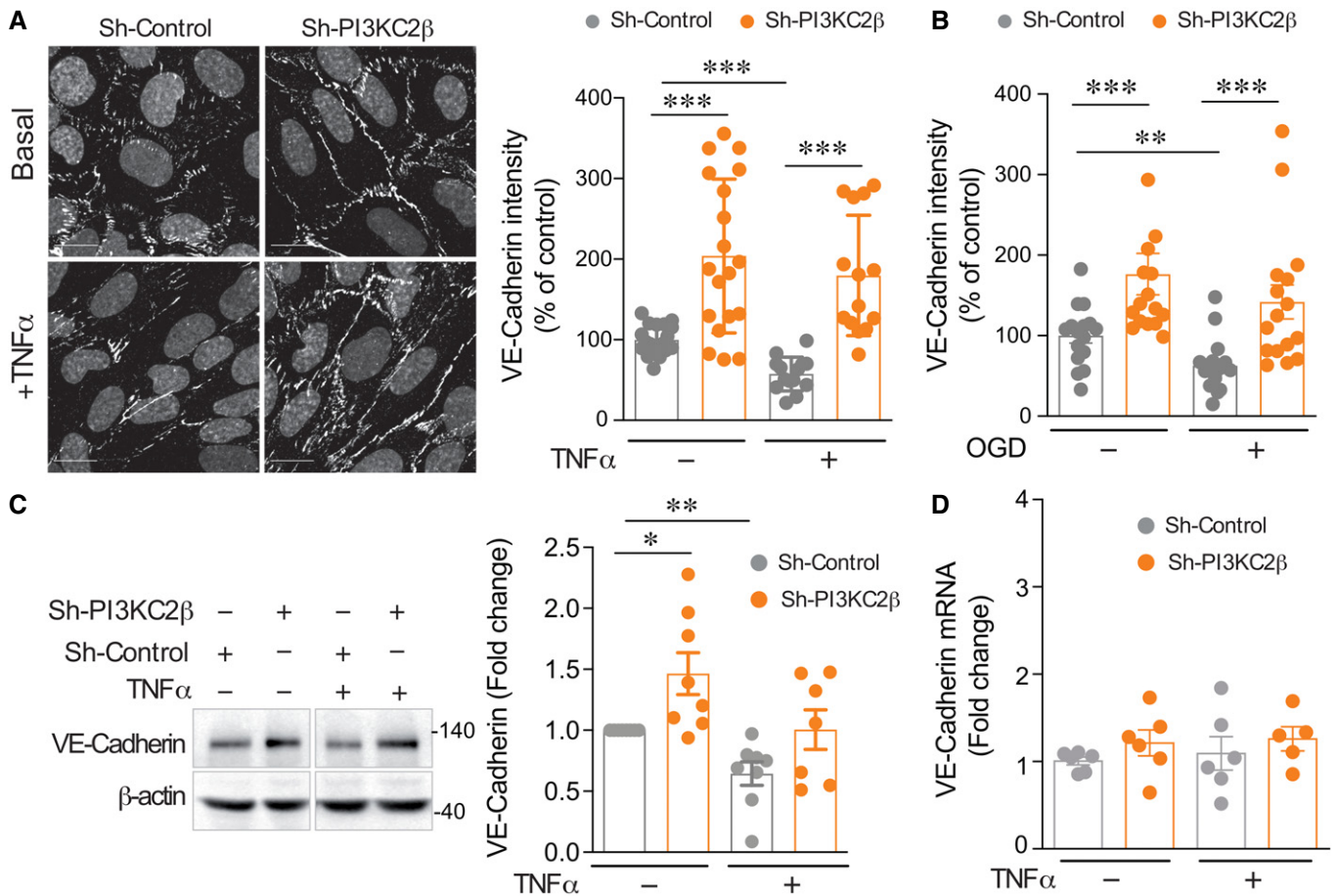


Figure 6. PI3KC2 β depletion increases the levels of VE-cadherin at the plasma membrane.

A Representative VE-cadherin staining and graph quantification of fluorescence intensity normalized to total number of cells per field (DAPI labeling) in sh-control and sh-PI3KC2 β hCMEC/D3 in resting condition and after 24 h activation with 25 ng/ml of TNF α . Control normalized to 100%. Scale bar, 15 μ m. Data represent mean \pm SEM of cell fields randomly selected (dots $n = 14$ –19). Data are collected from four to five independent experiments; *** $P < 0.001$, unpaired t-test.

B Graph quantification of fluorescence intensity of VE-cadherin normalized to total cell number per field (DAPI labeling) in control condition and after 5 h in oxygen-glucose deprivation (OGD) condition. Control normalized to 100%. Data represent mean \pm SEM of cell fields randomly selected (dots $n = 16$). Data were collected from five independent experiments; *** $P < 0.001$; ** $P < 0.01$, Mann-Whitney test.

C Representative Western blot and graph quantification of VE-cadherin from resting or activated (TNF α) cells. Lanes were run on the same gel but were noncontiguous. Densitometric measurements (mean \pm SEM) normalized to actin; control normalized to 1 ($n = 7$ –8 independent experiments); ** $P < 0.01$; * $P < 0.05$, one-sample t-test.

D Gene expression of VE-cadherin (*CDH5*) from sh-control and sh-PI3KC2 β hCMEC/D3 cells in resting condition or after 6 h of stimulation with TNF α . The mRNA levels are given as fold change to resting control hCMEC/D3 cells normalized to PGK1. Data represent mean \pm SEM of $n = 3$ independent experiments in duplicate; for sh-PI3KC2 β + TNF α , $n = 3$ independent experiments with only two experiments in duplicate. No significant changes between conditions were noted (Mann-Whitney test).

Source data are available online for this figure.

PI3KC2 β , decreased PI3P level by 81% (Appendix Fig S10D). Thus, Vps34 is the kinase that is mainly involved in the synthesis of PI3P in hCMEC/D3, and its inhibition in PI3KC2 β KD cells strongly reduced PI3P. The remaining amount of PI3P was probably due to other PI3K isoforms such as PI3KC2 α .

To determine if the catalytic activity of PI3KC2 β was involved in VE-cadherin accumulation at cell–cell junctions, a rescue experiment using membrane-permeant PI3P was performed. As shown in Appendix Fig S10C, the addition of exogenous PI3P resulted in a strong reduction of VE-cadherin at the plasma membrane of sh-PI3KC2 β cells, whereas no effect could be observed with exogenously added PI4P (used as a control) or PI

(3,4)P $_2$. Overall, these results suggest that VE-cadherin delivery to the adherens junctions is controlled by PI3KC2 β -dependent PI3P production.

We then tracked VE-cadherin trafficking by expressing VE-cadherin fused to citrin. Colocalization experiments revealed an increase in VE-cadherin–citrin in APPL1- and Rab11a-positive endosomes in PI3KC2 β -depleted cells (Fig 7C). Interestingly, PI3KC2 β -depleted cells transduced with a dominant-negative form of Rab11 (Rab11S25N) showed VE-cadherin levels comparable to control cells. This indicates that the absence of PI3KC2 β promoted VE-cadherin delivery to adherens junctions via Rab11 recycling endosomes (Fig 7D). Moreover, re-expression of PI3KC2 β in hCMEC/D3

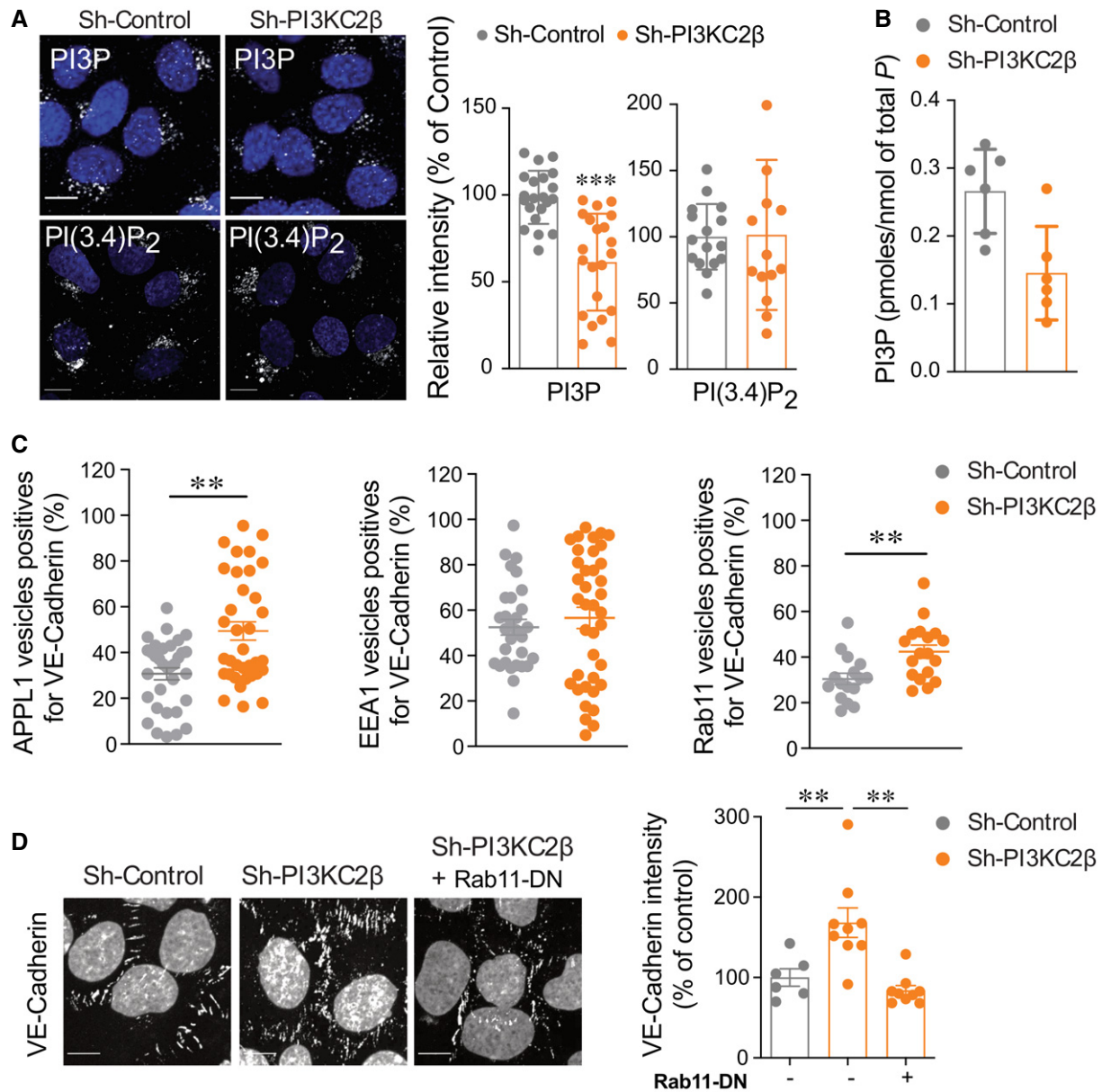


Figure 7. PI3KC2 β knockdown reduces VE-cadherin level in a Rab11a-dependent manner.

A Representative images of PI3P and PI(3,4)P₂ labeling and quantification using mCherry-FYVE^{HRS} and GFP-PH^(TAPP1) probes, respectively, in sh-control or sh-PI3KC2 β hCMEC/D3. Scale bar, 10 μ m. Nuclei are shown in blue (DAPI). Staining intensity was quantified by ImageJ software and normalized to total number of cells (DAPI labeling) per field. Data represent mean \pm SEM of cell fields randomly selected for PI3P (dots $n = 21$) and for PI(3,4)P₂ (dots $n = 14$ –16). Data were collected from at least five independent experiments; *** $P < 0.001$, unpaired t -test with Welch's correction.

B Quantification of total cellular PI3P levels in sh-control or sh-PI3KC2 β hCMEC/D3 cells by mass assay. Results are expressed as pmoles of PI3P/nmoles of total phosphore. Data represent mean \pm SD ($n = 2$ independent experiments in triplicate).

C Graph quantification of APPL1, EEA1, and Rab11 endosomes colocalized with mCitrin-VE-cadherin in sh-control and sh-PI3KC2 β hCMEC/D3 cells. Data are shown as percentage of total count endosomes per cell. Data are expressed as mean \pm SEM ($n = 33$ –35 cells for APPL1 and EEA1 endosomes and $n = 16$ –18 cells for Rab11 endosomes; three independent experiments); ** $P < 0.001$, Mann–Whitney test or unpaired t -test, as accordance.

D Representative confocal microscopic images of VE-cadherin immunostaining in sh-control cells, sh-PI3KC2 β cells or sh-PI3KC2 β cells transduced with Rab11S25N (Rab11-DN). Graph quantification of VE-cadherin; control normalized to 100%. Scale bar, 10 μ m. Data represent mean \pm SEM of cell fields randomly selected (dots $n = 6$ –9). Data are collected from at least three independent experiments; ** $P < 0.01$ Mann–Whitney test.

Source data are available online for this figure.

knockdown for PI3KC2 β rescued the phenotype with a decrease in APPL1- and Rab11-positive endosomes (Fig EV2A) and of VE-cadherin at the plasma membrane (Fig EV2B).

Collectively, these results indicate that loss of the PI3KC2 β favors VE-cadherin recycling pathway, presumably together with a decrease in its endocytosis, to increase its presence at adherens junctions.

Discussion

In this study, we identified class II PI3KC2 β as a potential target for modulating cerebrovascular permeability during stroke. Indeed, we provide evidence that PI3KC2 β inactivation has neuroprotective effects *in vivo* in two experimental stroke models. These two models are complementary and represent different clinical contexts with different post-ischemic reperfusion dynamics. Mechanical occlusion reversal by withdrawing the filament (tMCAO) results in prompt reperfusion, followed by post-ischemic hyperemia, mimicking interventional thrombectomy. In contrast, spontaneous or rtPA-accelerated reversal of thromboembolic occlusion gradually restores the circulation, which returns to normal after a longer interval (Orset *et al.*, 2007). Our results show that, in both cases, PI3KC2 β inactivation has a remarkable protective effect on endothelial junction disruption, infarct size, and inflammation.

Interestingly, following tMCAO, the inactivation of PI3KC2 β strongly reduced edema, infarct volumes, and the expression of soluble immune mediators. Moreover, only a few immune cells invaded the brain of C2 β ^{D121A/D1212A} mice after tMCAO. As a result, 24 h after tMCAO, C2 β ^{D121A/D1212A} mice exhibited a significant increase in survival, better global neurological function, and improved motor function and coordination. Similar results were obtained in the thromboembolic stroke model in which we used an ultrasensitive molecular MRI to show that the expression of P-selectin, a cerebrovascular inflammatory molecule expressed by endothelial cells, was significantly lower upon PI3KC2 β inactivation. Using BM chimera mice, we found that the inactivation of PI3KC2 β in the non-hematopoietic compartment is a key initiator of the *in vivo* protective effects, excluding a key role of PI3KC2 β in immune cells or in platelets. Moreover, data obtained on blood platelets discarded the role of this kinase activity in their activation, which is consistent with the absence of brain hemorrhagic phenotype in the knock-in animals.

In the tMCAO model, it is thought that brain damage largely occurs after recanalization due to ischemia-reperfusion injury. This is certainly less the case in the thromboembolic occlusion model where the recanalization process is slow and progressive. Our data show that in the tMCAO model, inflammatory signals are comparable after 1 h of ischemia in WT and C2 β ^{D121A/D1212A} mice, suggesting that PI3KC2 β inactivation mainly protects against the thromboinflammatory cascade during reperfusion in this model. However, the important protection observed in the thromboembolic occlusion model suggests that PI3KC2 β inhibition minimizes vascular injury even when the reperfusion is slow and gradual.

Our results clearly demonstrate the role of endothelial PI3KC2 β ; however, one cannot exclude a contribution of the microglia and astrocytes in the protective effect, although a potential role of this lipid kinase in these cells has not been described so far. Our data show that class II PI3KC2 β is a master regulator of the endosomal sorting machinery of VE-cadherin in human cerebral microvascular endothelial cells. PI3KC2 β knockdown distinctly enhanced the number of recycling endosomes, leading to an exacerbated VE-cadherin delivery to the plasma membrane, allowing junction integrity maintenance. Further, we show that PI3KC2 β is responsible for the production of a specific pool of PI3P in the early endosomal compartment regulating the endosomal flux. Indeed, a defect in the production of this specific pool of PI3P induced an accumulation of

very early endosomes (APPL1-positive vesicles) and a decrease of early (EEA1-positive vesicles) and late endosomes (LAMP1-positive vesicles). Our data also indicate an increase in the recycling pathway and, in turn, the enhanced presence of VE-cadherin at the plasma membrane and the maintenance of adherens junction integrity.

Other PI3Ks are known to produce PI3P in endothelial cells including PI3KC2 α , the close homologue of PI3KC2 β , and Vps34. PI3KC2 α has been shown to generate a PI3P pool required for the removal of recycling cargo from early endosomes. This pool was proposed to contribute to Rab11 activation (Campa *et al.*, 2018). However, our data suggest that PI3KC2 β generates a PI3P pool required for the conversion of very early endosomes (APPL1-positive) into early endosome (EEA1-positive), which is in line with previous reports in other cell models (Zoncu *et al.*, 2009; Alliouachene *et al.*, 2015). This mechanism has been described to be dependent on the small GTPase Rab5 (Zoncu *et al.*, 2009), whose localization to the endosomal compartment is reduced in hCMEC/D3 cells knockdown for PI3KC2 β . Thus, our results suggest that the pool of PI3P produced by PI3KC2 β contributes to the control of APPL1/EEA1 interconversion, possibly by interfering with Rab5 recruitment on the endosomal fraction. As a consequence, we observed a significant accumulation of APPL1-positive vesicles occurring at the expense of EEA1-positive endosomes. In addition, as PI3KC2 β -knockdown cells showed an increase in the recycling path through Rab11 activation, a local burst of PI3KC2 α activation cannot be excluded (Campa *et al.*, 2018).

Vps34 can also produce a pool of PI3P implicated in the trafficking machinery. Law *et al.* (2017) reported that the absence of the Vps34-dependent PI3P pool causes the enlargement of early endosomes as a consequence of Rab5 hyperactivity. These results suggest that the function of the two pools of PI3P generated either by Vps34 or by PI3KC2 β has distinct roles. While Vps34-dependent PI3P pool downregulates Rab5 activity via the recruitment of TBC-2 Rab GAP (Law *et al.*, 2017), our results suggest that the PI3KC2 β -dependent PI3P pool is rather involved in its endosomal localization, which could explain the opposite effect observed concerning the size of the early endosomes.

The reversal of the phenotype induced by expression of an inactivated form of Rab11 or by addition of exogenous cell-permeant PI3P in PI3KC2 β -knockdown cells supports the idea that loss of PI3KC2 β -dependent PI3P pool in cerebral endothelial cells increases the recycling pathway (Rab11a-positive endosomes) and enhances the presence of VE-cadherin at the plasma membrane and the maintenance of adherens junction integrity. This scenario is consistent with our *in vivo* results in mice expressing a catalytically inactive form of PI3KC2 β .

In human lung microvascular endothelial cells, Rab11a-positive endosomes have been shown to promote the restoration of junctional VE-cadherin localization via recycling to the plasma membrane (Yan *et al.*, 2016). In fact, depletion of Rab11a increased the colocalization of VE-cadherin with the LAMP1-positive lysosome, in both control and activated cells, resulting in persistent loss of adherent junctions and barrier integrity. Thus, Rab11a appears as a key regulator of VE-cadherin stabilization, by preventing its lysosomal degradation pathway. Altogether, our results and those from the literature strongly suggest that Rab11a-dependent recycling of endocytosed VE-cadherin favors vascular integrity following endothelial barrier dysfunction.

Recently, a pool of PI(3,4)P₂ produced by PI3KC2β on late endosomal/lysosomal membrane has been implicated in the repression of the mTORC1 pathway in nutrient deprivation conditions in HEK293T and HeLa cells (Marat *et al*, 2017; Wallroth *et al*, 2019). Thus, a reduced local production of PI(3,4)P₂ by PI3KC2β followed by its hydrolysis by the inositol polyphosphate 4-phosphatases (INPP4A or INPP4B) (Li & Marshall, 2015) could also alter the PI3P level. Although we cannot fully exclude the involvement of these 4-phosphatases, our study indicates that in cerebral endothelial cells, PI3KC2β knockdown significantly decreases PI3P level with no obvious effect on PI(3,4)P₂. Overall, these results suggest that according

to the cell model and physiological context, PI3KC2β can act on either PI(3,4)P₂ or PI3P and therefore regulate specific pathways.

This study demonstrates the remarkable ability of PI3KC2β inhibition to preserve VE-cadherin junction and BBB integrity under the conditions of extreme stress following ischemic stroke in mice. The striking protective effects observed in two stroke models of mice expressing an inactive form of PI3KC2β, the intermediate effect seen in heterozygous mice, and the absence of bleeding complications strongly suggest that small molecule inhibitors of this kinase (currently unavailable) could efficiently complement existing recanalization therapies.

Materials and Methods

Reagents and Tools table

Reagent/Resource	Reference or Source	Identifier or Catalog Number
Experimental Models		
PI3KC2β ^{D1212A/D1212A} C57BL/6J* C57BL/6NT (<i>M. musculus</i>)	B. Vanhaesebroeck (Alliouachene <i>et al</i> , 2015)	
hCMEC/D3 (<i>Homo sapiens</i>)	Tebubio (Weksler <i>et al</i> , 2005)	#CLU512-A
HMEC-1 (<i>Homo sapiens</i>)	ATCC (Ades <i>et al</i> , 1992)	CRL-3243
Recombinant DNA		
sh-Control	Sigma	SHC016
sh-PI3KC2β (1)	Sigma	TRCN0000002119
sh-PI3KC2β (2)	Sigma	TRCN0000002121
GFP-Rab11S25N	Addgene	#12678
GFP-PI3KC2β	V. Haucke	
N174 neomycin	Addgene	#81061
Antibodies		
Mouse-anti-PI3KC2β (monoclonal)	BD Biosciences	#611342
Mouse-anti-PI3KC2α (monoclonal)	BD Biosciences	#611046
Mouse-anti-VE-cadherin (monoclonal)	Santa Cruz	#9989 (F8)
Rabbit-anti-pS473-Akt (polyclonal)	Cell signaling	#4060 (D9E)
Rabbit-anti-Akt (polyclonal)	Cell signaling	#4691 (C67E7)
Rabbit-anti-pY204/pT202-ERK 1/2 (monoclonal)	Cell signaling	#4370 (D13.14.4E)
Rabbit-anti-ERK 1/2 (polyclonal)	Cell signaling	#9102
Rabbit-anti-pS235/236-S6 (monoclonal)	Cell signaling	#4858 (D57.2.2E)
Rabbit-anti-S6 (monoclonal)	Cell signaling	#2217 (5G10)
Rabbit-anti-HSP90 (monoclonal)	Cell signaling	#4877 (C45G5)
Mouse-anti-β-actin (monoclonal)	Sigma	#A2228 (AC74)
Goat-anti-rabbit	Promega	#W401B
Goat-anti-mouse	Promega	#W402B
Mouse-anti-VE-cadherin (monoclonal)	BD Biosciences	#555661
Rabbit-anti-APPL1 (monoclonal)	Ozyme	#3858S (D83H4)
Mouse-anti-EEA1 (monoclonal)	BD Biosciences	#610457
Mouse-anti-LAMP1 (monoclonal)	BD Biosciences	#555798
Rabbit-anti-Rab11a (polyclonal)	ThermoFischer	#71-5300
Rat-anti-Ly-6B.2 (monoclonal)	AbD Serotec	#MCA771GA
Goat-anti-P-Selectin (polyclonal)	R&D Systems	#AF737

Reagents and Tools table (continued)

Reagent/Resource	Reference or Source	Identifier or Catalog Number
Rat-anti-P-Selectin (monoclonal)	BD Biosciences	#553742 (RB40.34)
Other		
4-0 nylon monofilament	Docol	# 6023910PK10
Mice brain matrix	Stoelting	
Laser Doppler flowmetry system	FLPI	
Epithelial volt-ohmmeter	Merck Millipore	

Methods and Protocols

Animals

PI3KC2 β ^{D1212A/D1212A} kinase-dead knock-in mice and WT littermates bred on a C57BL/6 background were provided by B. Vanhaesebroeck (Alliouachene *et al*, 2015) and housed in the Anexplo (<http://anexplo.genotoul.fr>) vivarium according to institutional guidelines. Mice were housed in a 12-h light/dark cycle, in a humidity- and temperature-controlled ($22 \pm 2^\circ\text{C}$) environment with *ad libitum* access to food and water. All experiments were performed on 8–12 week-old mice (male and female).

Analysis of vessel density

One millimeter brain sections were fixed with PFA 3.7% during 1 h at 4°C , permeabilized 30 min with 0.1% triton, and then incubated with isolectin-B4 2 days. Brain section was imaged by confocal microscopy on a LSM 780 with $\times 20$ lens. Images were then analyzed using ImageJ software.

Ischemia model of tMCAO

Mice were anesthetized with 3% isoflurane in a mixture of 70% NO_2 and 30% O_2 for cerebral focal I/R induction by tMCAO. After midline neck incision, the internal carotid artery was occluded with a 4-0 nylon monofilament of 18 mm length (Docol, # 6023910PK10) with a flame-rounded tip to occlude the origin of the MCA. After 1 h of occlusion, mice were re-anesthetized, and the occluding filament was removed to allow for 24 h reperfusion (Braeuninger *et al*, 2012). Successful induction of focal ischemia was confirmed by contralateral hemiparesis. Exclusion criteria were excessive bleeding or death within 24 h after tMCAO.

Neurological assessment

Twenty-four hours after tMCAO, the modified Bederson score (Bederson *et al*, 1986) was used to determine global neurological function according to the following scoring system: 0, no deficit; 1, forelimb flexion; 2, decreased resistance to lateral push; 3, unidirectional circling; 4, longitudinal spinning; and 5, no movement. Motor function and coordination were evaluated by the grip test (Moran *et al*, 1995). For this test, the mouse was placed midway on a string between two supports and rated as follows: 0, falls off; 1, hangs onto string by one or both forepaws; 2, as for 1, and attempts to climb onto string; 3, hangs onto string by one or both forepaws plus one or both hindpaws; 4, hangs onto string by fore- and hindpaws plus tail wrapped around string; and 5, escape (to the support). Mice were randomly assigned to the operators. Steps for blinding of the investigators were taken to minimize the subjective bias when analyzing the data.

In vivo BBB leakage and brain edema

A 2% solution of Evans blue in saline was injected intravenously at 4 ml/kg into anesthetized mice (3% isoflurane in a mixture of 70% NO_2 and 30% O_2). Thirty minutes later, mice were anesthetized again. After cutting the right atrium, mice were perfused with saline through the left cardiac ventricle until the infusion fluid was colorless. The brains were removed, and 2-mm coronal sections were sliced for photography. The integrity of the BBB was assessed by measuring extravasation of Evans blue dye into the brain parenchyma. Planimetric measurements (ImageJ software, National Institutes of Health) were performed to evaluate brain edema.

Determination of infarct size

The brains of euthanized mice were harvested 24 h after tMCAO and cut into 2-mm coronal sections starting at 4 mm from the frontal pole using a mice brain matrix (Stoelting, Wood Dale, IL). The sections were stained by immersion in a 2% solution of 2,3,5-triphenyltetrazolium chloride (TTC; Sigma-Aldrich) in PBS (Sigma-Aldrich) for 10 min at room temperature (RT) to visualize the infarction. Infarct size was determined from digitized images by planimetric measurements (ImageJ software, National Institutes of Health) of the damaged area in the left (ipsilateral) hemisphere of each section normalized to the total area of the contralateral hemisphere. The results were corrected for brain edema as described in Ref. (Swanson *et al*, 1990).

Thromboembolic stroke model and electrocoagulation

The animals were anesthetized with isoflurane 5%, and anesthesia was maintained with 2.5% isoflurane in a 70%/30% mixture of NO_2/O_2 . Rectal temperature was controlled at $37 \pm 0.5^\circ\text{C}$ throughout the surgical procedure using a heating system. The mice were first placed in a stereotaxic device, the skin between the right eye and ear was incised, and the MCA was then exposed after a small craniotomy and dura mater excision. A micropipette filled with purified murine alpha-thrombin (0.05 mg; Stago BNL) was introduced into the MCA lumen, and 1 μl of thrombin (1.5 UI) was injected to induce *in situ* clot formation. The pipette was removed 10 min after occlusion (time required for clot stabilization) (Orset *et al*, 2007). The CBF was assessed using laser Doppler flowmetry system (FLPI, Oxford Optronix), with an optic fiber placed above the MCA territory before and up to 60 min after MCA occlusion.

MRI of brain lesions

Imaging was carried out on a PharmaScan 7 T/12 cm system using surface coils. T2*-weighted images were acquired to visualize

infarction using MSME sequences (multi-spin multi-echo): echo time/repetition time: 51 ms/2,500 ms with a $70 \mu\text{m} \times 70 \mu\text{m} \times 500 \mu\text{m}$ spatial resolution. Lesion sizes were measured 24 h post-surgery on T2-weighted images using ImageJ (v1.45 r, NIH).

Targeting moiety conjugation to MPIOs and molecular imaging

MPIOs (diameter $1.08 \mu\text{m}$) with *p*-toluenesulfonyl reactive surface groups (Invitrogen) were used for peptide conjugation (Montagne *et al*, 2012). Purified polyclonal goat anti-mouse antibodies for P-selectin (R&D Systems, #AF737) and purified monoclonal rat anti-mouse antibodies for P-selectin (BD Biosciences, #553742, clone RB40.34) were covalently conjugated to MPIOs in borate buffer with ammonium sulfate (pH 9.5), by incubation at 37°C for 48 h. Forty micrograms of targeting molecule (i.e., of each antibody) was used for the coating of 1 mg of reactive MPIOs. MPIOs were then washed in PBS containing 0.5% bovine serum albumin (BSA) at 4°C and incubated for 24 h at room temperature, to block the remaining active groups. MPIOs were rinsed in PBS (0.1% BSA) and stored at 4°C .

For contrast-enhanced MRI, a caudal catheter was placed and mice received intravenous injection of 2.0 mg Fe/kg of conjugated MPIOs (200 μl). Imaging was begun immediately after and lasted 20 min after particle administration. Three-dimension T2*-weighted gradient echo imaging with flow compensation (spatial resolution of $70 \mu\text{m} \times 70 \mu\text{m} \times 70 \mu\text{m}$ interpolated to an isotropic resolution of $70 \mu\text{m}$) with echo time/repetition time: 13.2 ms/200 ms and a flip angle of 21° was performed to visualize MPIOs (acquisition time: 20 min). All T2*-weighted images presented are minimum intensity projections of five consecutive slices (yielding a z-resolution of $350 \mu\text{m}$). Signal voids are quantified on 3D T2*-weighted images using automatic triangle threshold in ImageJ software (v1.45 r) (Gauberti *et al*, 2013). Results are presented as volume of MPIO-induced signal void divided by the volume of the structure of interest (in percent). The quality of conjugated MPIOs was systematically checked in a naïve mouse, by stereotaxic injection of lipopolysaccharide (1 μg in 1 μl) in the striatum (0.5 mm anterior, 2.0 mm lateral, and -3 mm ventral to the bregma).

Real-time quantitative polymerase chain reaction studies

Tissues were dissected and frozen. They were homogenized using a Precellys tissue homogenizer (Bertin Technology). The total RNA from tissues or hCMC cells was prepared using TRIzol reagent (Invitrogen, #15596026) and the GenElute Mammalian Total RNA Miniprep kit (Sigma-Aldrich, #RTN70-1KT). A total of 1 μg was reverse transcribed for 10 min at 25°C and 2 h at 37°C in a 20 μl final volume using the High Capacity cDNA Reverse Transcriptase Kit (Applied Biosystems, #4368814). Real-time quantitative polymerase chain reactions were performed using SsoFast EvaGreen Supermix (Bio-Rad, #1725201) on the StepOne instrument (Applied Biosystems). Primers are available on Appendix Table S2. Gene expression was quantified using the comparative threshold cycle method, TNF α , IL-1 β , IL-6, VE-cadherin, VCAM-1, RPS29, and PGK1 as control.

Enzyme-linked immunosorbent assays

Tissues were dissected and frozen. They were homogenized using a Precellys tissue homogenizer (Bertin Technology). Then, lysates were sonicated and centrifuged. TNF α , IL-6, and IL-1 β cytokines

present in the supernatant are quantified using ELISA kit (Thermo Fisher, #88-7324-22, # 88-7064-22, # 88-7013-22).

Immunohistochemistry

Front and rear portions of each brain that were post-fixed for 48 h (4% formaldehyde in PBS, 24 h, and then in 70% ethanol; Platform Anexplo Genotoul, Toulouse) or longer at room temperature in 10% neutral-buffered formalin (Sigma-Aldrich), embedded in paraffin, and sectioned at a thickness of $10 \mu\text{m}$. Tissue sections were mounted on pretreated slides and deparaffinized in xylene. Sections were incubated for 1 h in blocking buffer with 5% normal horse serum in phosphate-buffered saline (Sigma). Invading immune cells were detected by a rat anti-mouse Ly-6B.2 antibody (neutrophilic granulocytes; MCA771GA, 1:1,000; AbD Serotec). Negative controls for all histological experiments included omission of primary or secondary antibody and produced no signals (not shown).

Generation of bone marrow chimeric mice

The recipient mice from both genotypes (WT or C2 β ^{D1212A/D1212A} mice) were irradiated to the non-invasive exploration platform located at the Nuclear Medicine Department of the Rangueil Hospital (Biobeam Biological Irradiator 8000). The animals received a single dose of 9 Gray (Gy) for 6 min and their immune system rescued by BM transplantation from either WT or C2 β ^{D1212A/D1212A} donors after 24 h in ventilated cages with drinking water supplemented with 10% antibiotics Baytril (Bayer). The tMCAO surgery was performed 4 weeks later.

Tail bleeding time

Tail bleeding was measured by 3-mm tail-tip transection in anesthetized mice. A stopwatch was started immediately upon transection to determine the time required for the bleeding to three stop. Blood drops were removed every 15 s with the use of a paper filter. If bleeding did not recur within 30 s of cessation, it was considered stopped.

Preparation of washed mouse platelets and in vitro aggregation studies

Whole blood was drawn from the inferior vena cava of anesthetized mice (100 mg/kg ketamine, 10 mg/kg xylazine) into a syringe containing acid citrate dextrose (ACD; 1 vol anticoagulant/9 vol blood). To obtain an optimal amount of platelet-rich plasma (PRP), blood was mixed with one volume of modified HEPES-Tyrode's buffer (140 mmol/l NaCl, 2 mmol/l KCl, 12 mmol/l NaHCO₃, 0.3 mmol/l NaH₂PO₄, 1 mmol/l MgCl₂, 5.5 mmol/l glucose, 5 mmol/l HEPES, pH 6.7) containing 0.35% human serum albumin. After centrifugation at 150 g for 2 min at 37°C , PRP was removed and a further 300 μl of modified HEPES-Tyrode's buffer were added to the remaining blood, which was then centrifuged at 150 g for 2 min at 37°C . Then, PGI₂ at a final concentration of 500 nmol/l was added to the PRP, and platelets were pelleted by centrifugation at 1,000 g for 4 min at 37°C . Platelet pellets were finally resuspended in modified HEPES-Tyrode's buffer (pH 7.38) and pooled at a density of 5×10^8 platelets per ml in the presence of 0.02 unit/ml of the ADP scavenger apyrase (adenosine-5'-triphosphate diphosphohydrolase) and incubated for 45 min at 37°C before platelet stimulation. Aggregation was assessed using a Chrono-log dual channel aggregometer (Model 700) under stirring at 900 revolutions/min.

Cell culture

Immortalized human brain capillary endothelial cell line (hCMEC/D3) (Weksler *et al*, 2005; Daniels *et al*, 2013) was purchased from TebuBio (#CLU512-A). hCMEC/D3 cells were cultured at 37°C/5% CO₂ in rat tail collagen I (Cultrex rat collagen I, Trevigen, France)-coated plates (150 µg/ml) in EndoGRO MV complete culture media kit (Merck Millipore, #SCME004) at 2.5 × 10⁴ cells/cm². The cells were used until passage 35 for all experiments.

Knockdown of PI3KC2β by shRNA

Bacterial glycerol stocks containing the PI3KC2β shRNA (TRCN0000002119 and TRCN0000002121) or the pLKO.1-puro non-targeting shRNA control plasmid (SHC016) were purchased from Sigma-Aldrich (Appendix Table S1). hCMEC/D3 cells were transduced with lentiviral particles overnight and then incubated in fresh medium. Forty-eight hours after transduction, the cells were selected with puromycin (2 µg/ml, InvivoGen). At confluence, puromycin-resistant cells were FCS-starved overnight and then treated with TNFα (25 ng/ml, PeproTech, #300-01A), EGF (20 ng/ml; PeproTech, #315-09), exogenous membrane-permeant PI3P, PI4P, or PI(3,4)P₂ at 5 µM (Echelon: #P-3004; #P-4004; #P-3404) or Vps34-IN1 (Sigma-Aldrich, # 532628) at 1 µM during the indicated time.

hCMEC/D3 cell transduction

pLV-CDH5-mCitrin-IRES-puro and p-EGFP-C1-Rab11DN (S25N; serine 25 to asparagine) plasmid were purchased from Addgene (#85143, #12678). GFP-PI3KC2β was kindly provided by V. Haucke (Berlin, Germany). CDH5-mCitrin-, GFP-Rab11DN-, and GFP-PI3KC2β-encoding sequences were subcloned into N174-MCS (with neomycin resistance gene) lentiviral plasmid (Addgene, #81061) using In-Fusion HD Cloning Plus (Takara, #638909). N174-GFP-PI3KC2β was made resistant to the shRNA 2119 by site-directed mutagenesis (1126bp-cTcACcGTaGAcTTgCTc to 1126bp-gTcGAcCaGTcGAtTTaCTc) using In-Fusion HD Cloning Plus (Takara, #638909). hCMEC/D3 cells were transduced overnight by incubation with lentiviral particles and then incubated in fresh medium. Seventy-two hours after transduction, the cells were selected with G418 (250 µg/ml, Sigma). At confluence, neomycin-resistant cells were FCS-starved overnight and then treated or not with TNFα (25 ng/ml, PeproTech, #300-01A).

Oxygen and glucose deprivation experiment

At confluence, puromycin-resistant hCMEC/D3 cells were washed with PBS and the medium change for a DMEM glucose free (Thermo Fisher, #11966025) complemented with 1% penicillin/streptomycin and incubated at 37°C/5% CO₂/1% O₂ during 5 h. For control cells, the medium was change for a DMEM GlutaMAX (Gibco, #10566016) complemented with 20% SVF and 1% penicillin/streptomycin and cells incubated at 37°C/5% CO₂.

MitoSOX fluorescence imaging

The production of mitochondrial superoxide was monitored by fluorescence microscopy using the mitochondria-directed superoxide probe MitoSOX Red™ (Thermo Fisher, #M36008) according to the manufacturer's protocol. Briefly, cells were seeded at 2.5 × 10⁴ cells/cm² in collagen I-coated 48-well plates. After washes in PBS with Ca²⁺ and Mg²⁺, cells were kept in fresh medium containing MitoSOX Red™ (5 µmol/l; 15 min at 37°C). After washes, the

images were acquired using ×10 lens on ZOE™ fluorescent cell imager microscope.

Trans-endothelial electrical resistance

Trans-endothelial electrical resistance was performed as previously described (Chaitanya *et al*, 2011). Briefly, hCMEC/D3 cells were seeded on type I collagen pre-coated Transwell-Clear filters (Corning). The assay medium was changed after 4 and 7 days, and transport assays were performed when the cells formed monolayers (7–10 days after seeding). Insert culture systems were exposed to treatment (25 ng/ml hrTNFα, PeproTech #300-01A), and at different time points, resistance was measured using an epithelial volt-ohm-meter (Merck Millipore). The resistance of coated inserts was always subtracted from the resistance of endothelial cultures. The values obtained were plotted with GraphPad software (Prism) and checked for significance.

Transferrin trafficking

hCMEC/D3 cells on coverslips were preincubated overnight in serum-free medium. Cells were incubated with 20 µg/ml Alexa 546-labeled transferrin (Molecular Probes, #T23364) for 15 min at 4°C. Cells were washed with PBS and warmed to 37°C. At the different time points, cells were fixed in 4% formaldehyde 20 min at RT, incubated with DAPI (5 min) and mounted on glass slides with Mowiol mounting solution (Hoechst). The images were acquired using ×63 immersion lens on a LSM 780 confocal scanning microscope. Fluorescence intensity of three fields randomly selected per condition (normalized to cell number) for each experiment was analyzed by the ImageJ and Zen software.

Protein assay and immunoblot analysis

hCMEC/D3 cells were scrapped into buffer (20 mmol/l Tris pH 7.4; 150 mmol/l NaCl; 1 mmol/l EDTA; 1 mmol/l EGTA; 1 mmol/l β-Glycerophosphate; 2.5 mmol/l Na-Pyrophosphate; 1% Triton; 1% NP40; protease and phosphatase inhibitors). Then, lysates were sonicated and centrifuged. Proteins present in the supernatant are quantified by the method of BC Assay (Interchim #UP40840A) with Varioskan Flash (Thermo electron corporation). After denaturation in Laemmli sample buffer, samples were subjected to sodium dodecyl sulfate–polyacrylamide gel electrophoresis (SDS–PAGE) and transferred onto nitrocellulose membranes (Life Sciences). Membranes were blocked and incubated overnight at 4°C with respective primary antibody (see Reagents and Tools table) and then 2 h at room temperature with secondary antibody according to the manufacturer's instructions. Revelation was made using the ECL kit (Bio-Rad laboratories) by chemiluminescence. Immunoreactive bands were detected by the ChemiDoc MP Imager (Bio-Rad) device connected to the Image Lab software (version 4.0.1 build 6; Bio-Rad Laboratories) allowing the densitometric analysis with ImageJ software.

PI3P quantification by mass assay

Cell extract for mass assay was prepared as follows. After removing the media, the cells were immediately scraped on ice with ice-cold 1 mol/l HCl, followed by centrifugation at 751 g at 4°C, and the cell pellet was snap-frozen. The samples were stored at –80°C before processing for PI3P mass assay as previously described (Chicanne *et al*, 2012).

GST-mCherry-FYVE^{HRS} and GST-EGFP-PH^{Tapp1} probes

The pGEX-4T1-mCherry-FYVE^{HRS} and pGEX-4T1-EGFP-PH^{Tapp1} plasmids were transformed into *Escherichia coli* BL21(DE3). Single colony was used to prepare a starter culture that was expanded and grown at 37°C until O.D. 600 nm reaches 0.6–0.8. The expression of the recombinant proteins was induced with 0.5 mM IPTG overnight at 18°C. After centrifugation, bacterial pellets were lysed in a cold buffer containing 50 mM Tris pH 7.5, 150 mM NaCl, 1% Triton X-100, 5 mM DTT, 10% glycerol containing protease inhibitor cocktail and 0.5 mg/ml lysozyme. Following sonication and centrifugation, GST-mCherry-FYVE^{HRS} and GST-EGFP-PH^{Tapp1} were purified with Glutathione-Sepharose 4B beads, eluted with 20 mM reduced glutathione, dialyzed, concentrated, and analyzed by SDS-PAGE and Coomassie staining.

Confocal imaging

Cells were fixed 20 min in 4% formaldehyde. For VE-cadherin labeling, cells were permeabilized with 0.1% Triton X-100. Cells were blocked and incubated 2 h at RT with primary antibodies (available on Reagents and Tools table) and then 1 h at RT with the appropriate fluorescent secondary antibody.

For endosomal compartments, cells were permeabilized with 0.5% saponin and blocked with 1% BSA and 0.05% saponin.

For probe staining, cells were fixed 10 min in 4% formaldehyde and rinsed with 50 mmol/l solution of glycine in PIPES buffer (137 mmol/l NaCl; 2.7 mmol/l KCl; 20 mmol/l PIPES pH 6.8). Permeabilization was carried out with digitonin (20 µM). Lamellae were incubated with recombinantly expressed mCherry-FYVE^{HRS} (50 µg/ml) or GFP-PH^(TAPP1) (5 µg/ml) probes directed against PI3P and PI(3,4)P₂, respectively, and post-fixed in 4% formaldehyde. Cell nuclei (blue) were labeled with DAPI.

Coverslips were mounted on glass slides with Mowiol mounting solution (Hoechst). The images were acquired using ×63 immersion lens on a LSM 780 confocal scanning microscope, and the data were analyzed by the ImageJ and Zen software. For each experiment, three to four randomly selected fields (plots on the histograms) per condition were quantified and normalized to total cell number per field according to DAPI nucleus labeling (each field contained an average of 20 cells). Three to five independent experiments were performed.

OptiPrep gradient fractionation

Cells were plated at a density of 2.5×10^4 cells/cm² in collagen I-coated 150 mm dishes and grown to confluence. After washes with PBS and SIM buffers (250 mmol/l sucrose, 3 mmol/l imidazole and 1 mmol/l MgCl₂ pH 7.4), pellets were resuspended in SIM buffer with 1 mmol/l DTT and protease inhibitors and broken in ball-bearing homogenizer. Cell homogenates were centrifuged 20 min at 2,000 g at 4°C, and supernatant was collected. Then, supernatant was adjusted to 40.6% in OptiPrep dilution buffer (235 mmol/l KCl, 12 mmol/l MgCl₂, 25 mmol/l CaCl₂, 30 mmol/l EGTA, 150 mmol/l HEPES-NaOH pH 7.0) and loaded at the bottom of 5–20% OptiPrep gradient previously made using a Gradient Master. The loaded gradient was ultracentrifuged using a SW41 Ti rotor (Beckman) at 100,000 g during 20 h at 4°C. Equal fractions of gradient were collected and centrifuged 45 min at 110,000 g. Fractions were denatured in Laemmli sample buffer, subjected to SDS-PAGE, and transferred onto nitrocellulose membranes (Life Sciences). Then, immunoblot protocol was used.

GTP-agarose bead pull-down assay

The GTP loading activities of Rab5, Rab7, and Rab11 GTPases were monitored by pull-down assay using GTP-agarose beads (Kim *et al*, 2017). Cells were plated at a density of 2.5×10^4 cells/cm² in collagen I-coated 100-mm dishes and grown to confluence. After washes with PBS, cells were lysed in GTP-binding buffer (20 mM Tris-HCl pH 7.5, 5 mM MgCl₂, 2 mM PMSF, 20 µg/ml leupeptin, 10 µg/ml aprotinin, 150 mM NaCl, 1% Triton X-100). Cell homogenates were sonicated and centrifuged 10 min at 13,000 g at 4°C. Supernatant was collected and incubated overnight with precleared GTP-agarose beads in the absence or presence of GTP in excess (200 µM). Beads were then washed with the GTP-binding buffer, and proteins were eluted by boiling in reducing Laemmli sample buffer. SDS-PAGE and Western blot followed, as above.

Statistics

All data are shown as mean ± SEM. The difference between means was calculated by one-way and two-way ANOVA, unpaired *t*-test, one-sample *t*-test, or corresponding nonparametric test (as appropriate and determined by D'Agostino & Pearson omnibus normality test) and complemented with post-test when needed. Statistical significance was set at $P < 0.05$ and indicated as * $P < 0.05$, ** $P \leq 0.01$, and *** $P \leq 0.001$ using Prism Software (GraphPad, version 5 or 6).

Study approval

All animal procedures were performed in accordance with the guidelines of the Ethics Committee on Animal Experimentation and with the regulations of the French Ministry of Agriculture (<http://anexplo.genotoul.fr>).

Data availability

This study includes no data deposited in external repositories.

Expanded View for this article is available online.

Acknowledgements

The authors thank the personnel of Anexplo animal facilities (US006/CREFRE Inserm/UPS) for animal handling and Genotoul Imaging facilities (INSERM U1048) for expert technical assistance. This work was supported by Inserm, ANR (No. ANR-16-CE14-0009-01), and Fondation pour la Recherche Médicale (FRM grant number DEQ20170336737). T.A. was supported by ANR (No. ANR-16-CE14-0009-01) and the Nouvelle Société Française d'Athérosclérose (NSFA, 2019); R.S. was supported by Fondation de France (grant 00056850). B.P. is a scholar of the Institut Universitaire de France.

Author contributions

TA, RS, AJ, and JD performed most experiments and analyzed data; TA and RS maintained mouse colonies. GC designed and performed lentiviral transduction and phosphoinositide analysis; KH designed and performed Opti-Prep gradient fractionation and GTPases activity; JV provided reagent and lipid probes; CO and DV designed and performed thromboembolic stroke model and MRI analysis; EG and CK participated to the setting of tMCAO model in the laboratory; BV produced the mice; M-PG designed research and supervised the work. M-PG, BP, and VL analyzed the data. M-PG, BV, and BP wrote the manuscript.

Conflict of interest

B.V. is a consultant for Karus Therapeutics (Oxford, UK), iOnctura (Geneva, Switzerland), and Venthera (Palo Alto, US) and has received speaking fees from Gilead. The other authors have no competing financial interest to declare.

References

- Ades EW, Candal FJ, Swerlick RA, George VG, Summers S, Bosse DC, Lawley TJ (1992) HMEC-1: establishment of an immortalized human microvascular endothelial cell line. *J Invest Dermatol* 99: 683–690
- Alliouachene S, Bilanges B, Chicanne G, Anderson KE, Pearce W, Ali K, Valet C, Posor Y, Low PC, Chaussade C et al (2015) Inactivation of the class II PI3K-C2beta potentiates insulin signaling and sensitivity. *Cell Rep* 13: 1881–1894
- Bederson JB, Pitts LH, Tsuji M, Nishimura MC, Davis RL, Bartkowski H (1986) Rat middle cerebral artery occlusion: evaluation of the model and development of a neurologic examination. *Stroke* 17: 472–476
- Bilanges B, Posor Y, Vanhaesebroeck B (2019) PI3K isoforms in cell signalling and vesicle trafficking. *Nat Rev* 20: 515–534
- Braeuninger S, Kleinschnitz C, Nieswandt B, Stoll G (2012) Focal cerebral ischemia. *Methods Mol Biol* 788: 29–42
- Campa CC, Margaria JP, Derle A, Del Giudice M, De Santis MC, Gozzelino L, Copperi F, Bosia C, Hirsch E (2018) Rab11 activity and PtdIns(3)P turnover removes recycling cargo from endosomes. *Nat Chem Biol* 14: 801–810
- Chaitanya GV, Cromer WE, Wells SR, Jennings MH, Couraud PO, Romero IA, Weksler B, Erdreich-Epstein A, Mathis JM, Minagar A et al (2011) Gliovascular and cytokine interactions modulate brain endothelial barrier *in vitro*. *J Neuroinflammation* 8: 162
- Chicanne G, Severin S, Boscheron C, Terrisse AD, Gratacap MP, Gaits-iacovoni F, Tronchere H, Payraastre B (2012) A novel mass assay to quantify the bioactive lipid PtdIns3P in various biological samples. *Biochem J* 447: 17–23
- Chikh A, Ferro R, Abbott JJ, Pineiro R, Buus R, Iezzi M, Ricci F, Bergamaschi D, Ostano P, Chiorino G et al (2016) Class II phosphoinositide 3-kinase C2beta regulates a novel signaling pathway involved in breast cancer progression. *Oncotarget* 7: 18325–18345
- Daniels BP, Cruz-Orengo L, Pasiaka TJ, Couraud PO, Romero IA, Weksler B, Cooper JA, Doering TL, Klein RS (2013) Immortalized human cerebral microvascular endothelial cells maintain the properties of primary cells in an *in vitro* model of immune migration across the blood brain barrier. *J Neurosci Methods* 212: 173–179
- Dejana E, Vestweber D (2013) The role of VE-cadherin in vascular morphogenesis and permeability control. *Prog Mol Biol Transl Sci* 116: 119–144
- Esenwa C, Gutierrez J (2015) Secondary stroke prevention: challenges and solutions. *Vasc Health Risk Manag* 11: 437–450
- Gauberti M, Montagne A, Marcos-Contreras OA, Le Behot A, Maubert E, Vivien D (2013) Ultra-sensitive molecular MRI of vascular cell adhesion molecule-1 reveals a dynamic inflammatory penumbra after strokes. *Stroke* 44: 1988–1996
- Giannotta M, Trani M, Dejana E (2013) VE-cadherin and endothelial adherens junctions: active guardians of vascular integrity. *Dev Cell* 26: 441–454
- Gulluni F, De Santis MC, Margaria JP, Martini M, Hirsch E (2019) Class II PI3K functions in cell biology and disease. *Trends Cell Biol* 29: 339–359
- Hacke W, Kaste M, Bluhmki E, Brozman M, Dávalos A, Guidetti D, Larrue V, Lees KR, Medeghri Z, Machnig T et al (2008) Thrombolysis with alteplase 3 to 4.5 hours after acute ischemic stroke. *N Engl J Med* 359: 1317–1329
- Harada K, Truong AB, Cai T, Khavari PA (2005) The class II phosphoinositide 3-kinase C2beta is not essential for epidermal differentiation. *Mol Cell Biol* 25: 11122–11130
- Iadecola C, Anrather J (2011) The immunology of stroke: from mechanisms to translation. *Nat Med* 17: 796–808
- Kim JH, Lee C, Lee M, Wang H, Kim K, Park SJ, Yoon I, Jang J, Zhao H, Kim HK et al (2017) Control of leucine-dependent mTORC1 pathway through chemical intervention of leucyl-tRNA synthetase and RagD interaction. *Nat Commun* 8: 732
- Konsman JP, Drukarch B, Van Dam AM (2007) (Peri)vascular production and action of pro-inflammatory cytokines in brain pathology. *Clin Sci (Lond)* 112: 1–25
- Lambertsen KL, Finsen B, Clausen BH (2019) Post-stroke inflammation-target or tool for therapy? *Acta Neuropathol* 137: 693–714
- Law F, Seo JH, Wang Z, DeLeon JL, Bolis Y, Brown A, Zong WX, Du G, Rocheleau CE (2017) The VPS34 PI3K negatively regulates RAB-5 during endosome maturation. *J Cell Sci* 130: 2007–2017
- Li H, Marshall AJ (2015) Phosphatidylinositol (3,4) bisphosphate-specific phosphatases and effector proteins: a distinct branch of PI3K signaling. *Cell Signal* 27: 1789–1798
- Marat AL, Wallroth A, Lo WT, Muller R, Norata GD, Falasca M, Schultz C, Hauke V (2017) mTORC1 activity repression by late endosomal phosphatidylinositol 3,4-bisphosphate. *Science (New York, NY)* 356: 968–972
- Mavrommati I, Cisse O, Falasca M, Maffucci T (2016) Novel roles for class II phosphoinositide 3-Kinase C2beta in signalling pathways involved in prostate cancer cell invasion. *Sci Rep* 6: 23277
- Montagne A, Gauberti M, Macrez R, Jullienne A, Briens A, Raynaud J-S, Louin G, Buisson A, Haelewyn B, Docagne F et al (2012) Ultra-sensitive molecular MRI of cerebrovascular cell activation enables early detection of chronic central nervous system disorders. *NeuroImage* 63: 760–770
- Moran PM, Higgins LS, Cordell B, Moser PC (1995) Age-related learning deficits in transgenic mice expressing the 751-amino acid isoform of human beta-amyloid precursor protein. *Proc Natl Acad Sci USA* 92: 5341–5345
- Nigorikawa K, Hazeki K, Guo Y, Hazeki O (2014) Involvement of class II phosphoinositide 3-kinase alpha-isoform in antigen-induced degranulation in RBL-2H3 cells. *PLoS One* 9: e111698
- Orset C, Macrez R, Young AR, Panthou D, Angles-Cano E, Maubert E, Agin V, Vivien D (2007) Mouse model of *in situ* thromboembolic stroke and reperfusion. *Stroke* 38: 2771–2778
- Posor Y, Eichhorn-Gruenig M, Puchkov D, Schöneberg J, Ullrich A, Lampe A, Müller R, Zerbakhsh S, Gulluni F, Hirsch E et al (2013) Spatiotemporal control of endocytosis by phosphatidylinositol-3,4-bisphosphate. *Nature* 499: 233–237
- Quenault A, Martinez de Lizarrondo S, Etard O, Gauberti M, Orset C, Haelewyn B, Segal HC, Rothwell PM, Vivien D, Touzé E et al (2017) Molecular magnetic resonance imaging discloses endothelial activation after transient ischaemic attack. *Brain* 140: 146–157
- Swanson RA, Morton MT, Tsao-Wu G, Savalos RA, Davidson C, Sharp FR (1990) A semiautomated method for measuring brain infarct volume. *J Cereb Blood Flow Metab* 10: 290–293
- Tibolla G, Pineiro R, Chiozzotto D, Mavrommati I, Wheeler AP, Norata GD, Catapano AL, Maffucci T, Falasca M (2013) Class II phosphoinositide 3-kinases contribute to endothelial cells morphogenesis. *PLoS One* 8: e53808
- Wallroth A, Koch PA, Marat AL, Krause E, Hauke V (2019) Protein kinase N controls a lysosomal lipid switch to facilitate nutrient signalling via mTORC1. *Nat Cell Biol* 21: 1093–1101

- Weksler Bb, Subileau Ea, Perrière N, Charneau P, Holloway K, Leveque M, Tricoire-Leignel H, Nicotra A, Bourdoulous S, Turowski P et al (2005) Blood-brain barrier-specific properties of a human adult brain endothelial cell line. *FASEB J* 19: 1872–1874
- Weksler B, Romero IA, Couraud PO (2013) The hCMEC/D3 cell line as a model of the human blood brain barrier. *Fluids Barriers CNS* 10: 16
- Wessel F, Winderlich M, Holm M, Frye M, Rivera-Galdos R, Vockel M, Linnepe R, Ipe U, Stadtmann A, Zarbock A et al (2014) Leukocyte extravasation and vascular permeability are each controlled *in vivo* by different tyrosine residues of VE-cadherin. *Nat Immunol* 15: 223–230
- Xiong Y, Mahmood A, Chopp M (2010) Angiogenesis, neurogenesis and brain recovery of function following injury. *Curr Opin Investig Drugs* 11: 298–308
- Yan Z, Wang ZG, Segev N, Hu S, Minshall RD, Dull RO, Zhang M, Malik AB, Hu G (2016) Rab11a mediates vascular endothelial-cadherin recycling and controls endothelial barrier function. *Arterioscler Thromb Vasc Biol* 36: 339–349
- Yang C, Hawkins KE, Dore S, Candelario-Jalil E (2019) Neuroinflammatory mechanisms of blood-brain barrier damage in ischemic stroke. *Am J Physiol* 316: C135–C153
- Yoshioka K, Yoshida K, Cui H, Wakayama T, Takuwa N, Okamoto Y, Du W, Qi X, Asanuma K, Sugihara K et al (2012) Endothelial PI3K-C2alpha, a class II PI3K, has an essential role in angiogenesis and vascular barrier function. *Nat Med* 18: 1560–1569
- Zoncu R, Perera RM, Balkin DM, Pirruccello M, Toomre D, De Camilli P (2009) A phosphoinositide switch controls the maturation and signaling properties of APPL endosomes. *Cell* 136: 1110–1121